Assessing the impact of relative permeability and capillary heterogeneity on Darcy flow modelling of CO 2 storage in Utsira Formation

Onoja, M. U. & Shariatipour, S. M.

Original citation & hyperlink:
Onoja, MU & Shariatipour, SM 2019, 'Assessing the impact of relative permeability and capillary heterogeneity on Darcy flow modelling of CO 2 storage in Utsira Formation' Greenhouse Gases: Science and Technology, vol. 9, no. 6, https://doi.org/10.1002/ghg.1932, pp. 1221-1246. https://dx.doi.org/10.1002/ghg.1932

DOI 10.1002/ghg.1932
ESSN 2152-3878

Publisher: Wiley

Assessing the impact of relative permeability and capillary heterogeneity on Darcy flow modelling of CO_2 storage in Utsira Formation

Michael U. Onoja[a]* and Seyed M. Shariatipour[a]

[a]Centre for Fluid and Complex Systems, Maudslay House, Coventry University, Coventry, CV1 2NL, United Kingdom

*Corresponding author: onojau@coventry.ac.uk

This is the accepted version of the following article:

Onoja, M. U. and Shariatipour, S. M. (2019), Assessing the impact of relative permeability and capillary heterogeneity on Darcy flow modelling of CO_2 storage in Utsira Formation. *Greenhouse Gas Sci Technol*. doi:10.1002/ghg.1932

which has been published in final form at doi:10.1002/ghg.1932. This article may be used for non-commercial purposes in accordance with the Wiley Self-Archiving Policy [http://www.wileyauthors.com/self-archiving].

Abstract

Predicting CO_2 plume migration is an important aspect for the geological sequestration of CO_2. In the absence of experimental data, the storage performance of CO_2 geo-storage can be assessed through the dynamic modelling of the fluid flow and transport properties of the rock-fluid system using empirical formulations. Using the van Genuchten empirical model, this study documents a Darcy flow modelling approach to investigate different aspects of CO_2 drainage in a sandstone formation with interbedded argillaceous (*i.e.* mudstone) units. The numerical simulation is based on the Sleipner Gas Field storage unit where several thin argillite layers occur within the sandstone of the Utsira Formation. With respect to forward modelling simulations that have used Sleipner Formation as a case study, it is noted that previous attempts to numerically calibrate the CO_2 plume migration to time-lapse seismic dataset using software governed by Darcy flow physics achieved poor results. In this study, CO_2-brine buoyant displacement pattern is simulated using the ECLIPSE 'black oil' simulator within a two-dimensional (2D) axisymmetric geometry and a three-dimensional (3D) Cartesian coordinate system. This investigation focused on two key parameters affecting CO_2 migration mobility, namely relative permeability and capillary forces. Examination of these parameters indicate that for the gravity current of CO_2 transiting through a heterogeneous siliciclastic formation, the local capillary forces in geologic units, such as mudstone and sandstones, and the relative permeability to the invading fluid control the mass of CO_2 that breaches and percolates through each unit, respectively. In numerical analysis, these processes influence the evaluation of structural and residual trapping mechanisms. Consequently, the inclusion of heterogeneities in capillary pressure and relative permeability functions, where and when applicable, advances a Darcy modelling approach to history matching and forecasting of reservoir performance. Results indicate that there is a scope for a revision of the basic premise for modelling flow properties in the interbedded mudstones and the top sand wedge at the Sleipner Field when using Darcy flow simulators.

Keywords: Capillary heterogeneity; CO_2 sequestration; Darcy flow analysis; Numerical modelling and simulation; Relative permeability heterogeneity.

1 Introduction

Sedimentological processes such as variation in grain size and sorting can result in relative permeability and capillary heterogeneity in a geological formation.[1] Such heterogeneities are a source of uncertainty in CO_2 storage performance because they influence fluid flow paths and the position of flow units within the reservoir formation.

Bear[2] defined the concept of flow unit as the representative elementary volume (REV) or mappable portion of the reservoir which possess analogous petrophysical properties that affect fluid flow and differ from other sections of the reservoir rock volume. Although the accurate characterisation of flow units in a reservoir formation helps to reduce the uncertainty in CO_2 sequestration and oil production forecast,[3,4] many reservoir simulation studies overlook relative permeability and capillary heterogeneity in dynamic flow modelling. Such practice could introduce further uncertainty in the assessment of dynamic flow processes during CO_2 injection.

A typical reservoir rock with mudstone intervals contains varying amount of clay minerals,[5] which can result in different flow units for CO_2 storage. To this end, this study identifies the effect of incorporating heterogeneity in relative permeability and capillary pressure functions on Darcy flow analysis of CO_2 storage performance in a heterogeneous siliciclastic formation. As a case study, an overview of Darcy flow analysis of CO_2 injection is centred on the Utsira Formation of the Sleipner reservoir unit[6] (a good example of a sandstone formation with interbedded mudstones).

The Utsira Formation in the Norwegian North Sea is a saline aquifer that lies at a depth of 800 m below sea level (mbsl).[6] It is a 200 – 300m thick sandstone formation in the Sleipner area overlain by 50 – 100m thick 'shale' of the Nordland Group, acting as the primary reservoir caprock, and underlain by the Hordaland Group (Figure 1). The Utsira Sand is mostly unconsolidated and largely uncemented with no evidence of faults. It has an average porosity of 36% and a

permeability range from 1000 and 8000 mD.[7] Geophysical well logs acquired around the Sleipner area show laterally extensive thin beds of argillite within the Utsira Formation, about 1 – 1.5 m thick, and a 5 – 6.5 m thick argillaceous layer separating an eastward thickening sand body, commonly referred to as the 'sand wedge', from the underlying Utsira Sand[7]. These interbedded mudstone layers are characterised by spikes of higher gamma readings which are similar to those of the overlying Nordland Shale.

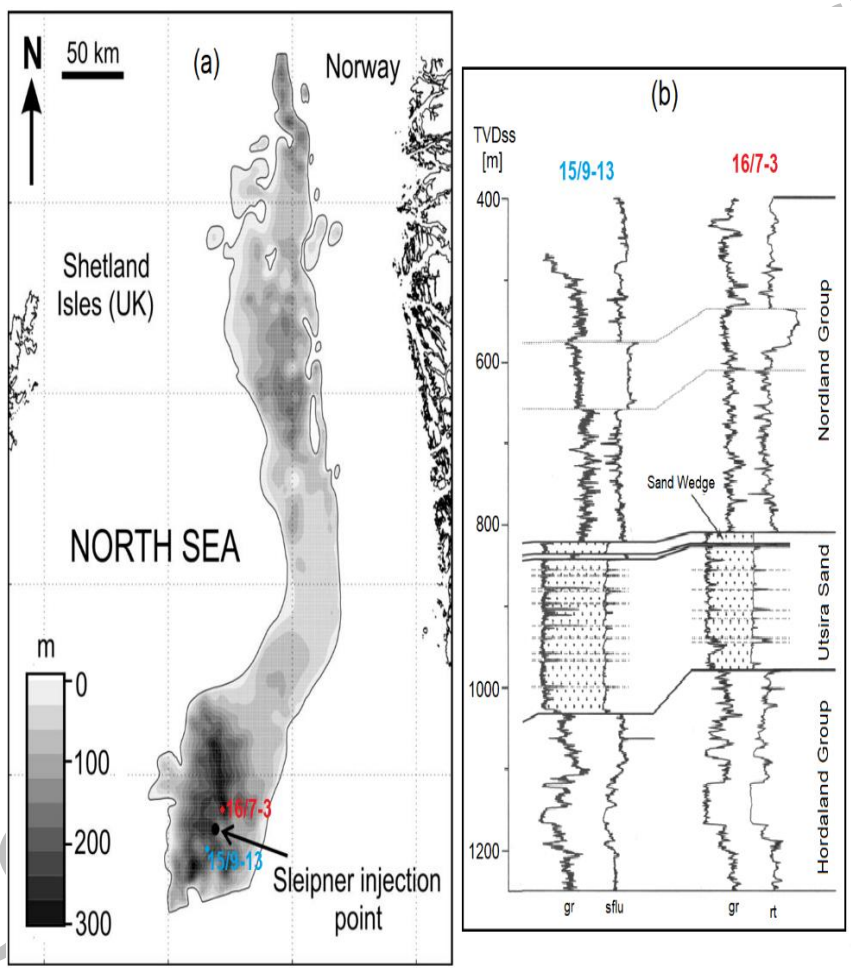

Figure 1. a) Isopach map of the Utsira Sand showing the Sleipner injection point and two surround wells and b) representative geophysical well logs showing the Utsira Sand characterised by generally low gamma-ray and low resistivity values. [Adapted from Chadwick et al.,[8]]

CO_2 injection began in the Sleipner reservoir unit in 1996 at an average annual rate of 1 Mt. A time-lapse monitoring programme was initiated in 1994 to monitor the migration and dispersal of the CO_2 plume. Interpretations of the seismic reflection surveys show that by 1999, three years after injection commenced, the Sleipner CO_2 plume had breached the mudstone barriers within the

Utsira Sand and ascended from the injection point to the reservoir-caprock interface via nine reflective layers (Figure 2).

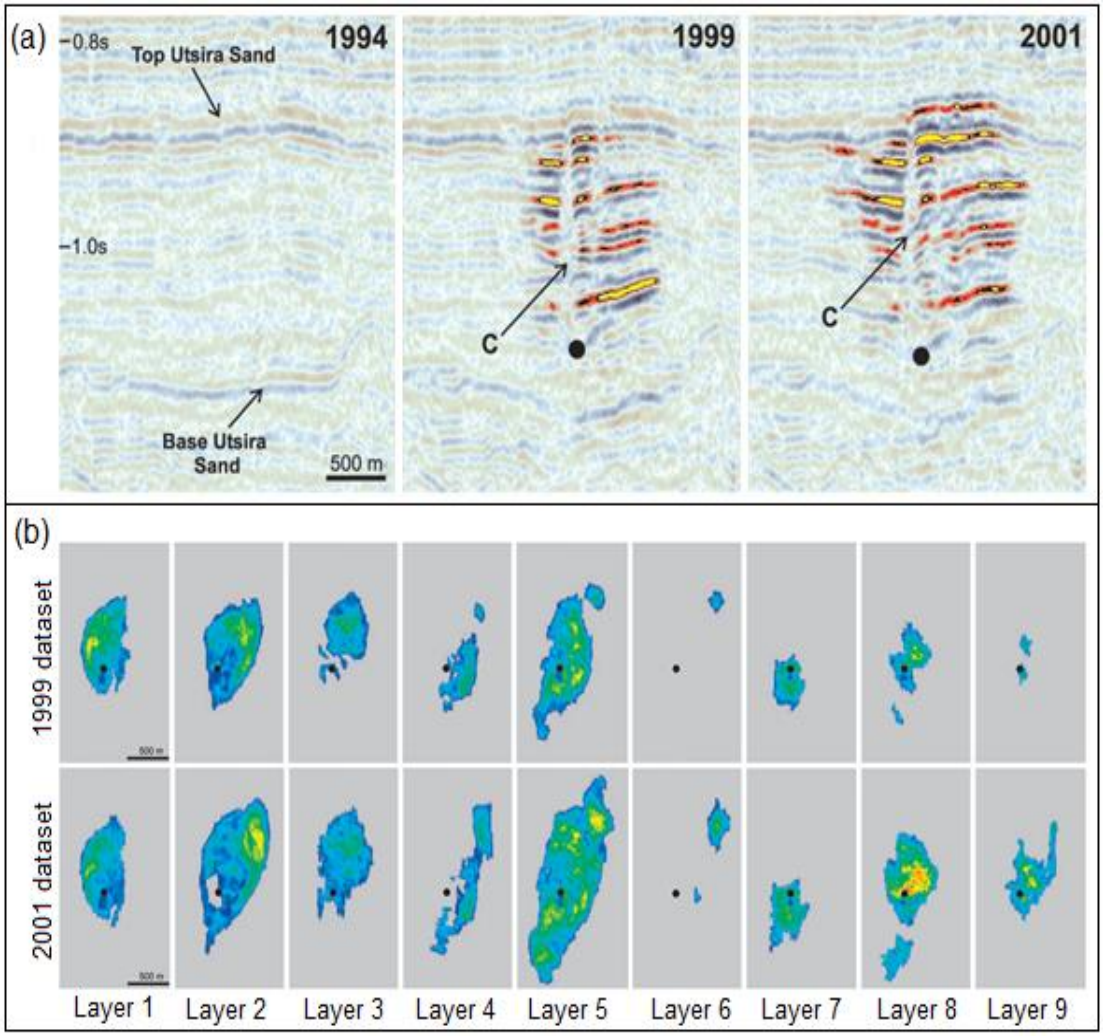

Figure 2: a) Time-lapse seismic images of the CO_2 plume N-S inline through 1994 (prior to injection), 1999 and 2001 datasets with C denoting the main chimney and the solid circle depicting the injection point. b) Absolute amplitude maps of the interpreted layers showing plume development in the 1999 and 2001 seismic surveys. Black disc denotes injection point. [Adapted from Chadwick et al.,[8]].

In Figure 2a, the vertical zones within the plume, annotated by C, are interpreted as the main conduit for CO_2 upward migrated and referred to as chimneys.[9] Of all nine layers, the top layer is imaged most clearly by the seismic surveys. This top layer of CO_2 accumulation is the sand wedge (Figure 1b) and it is regarded as the main determinant of storage integrity in the medium to longer term.[10] A north-trending linear propagation of the layer is particularly prominent and corresponds to CO_2 migrating northwards along a linear ridge at the reservoir top (Figure 3).

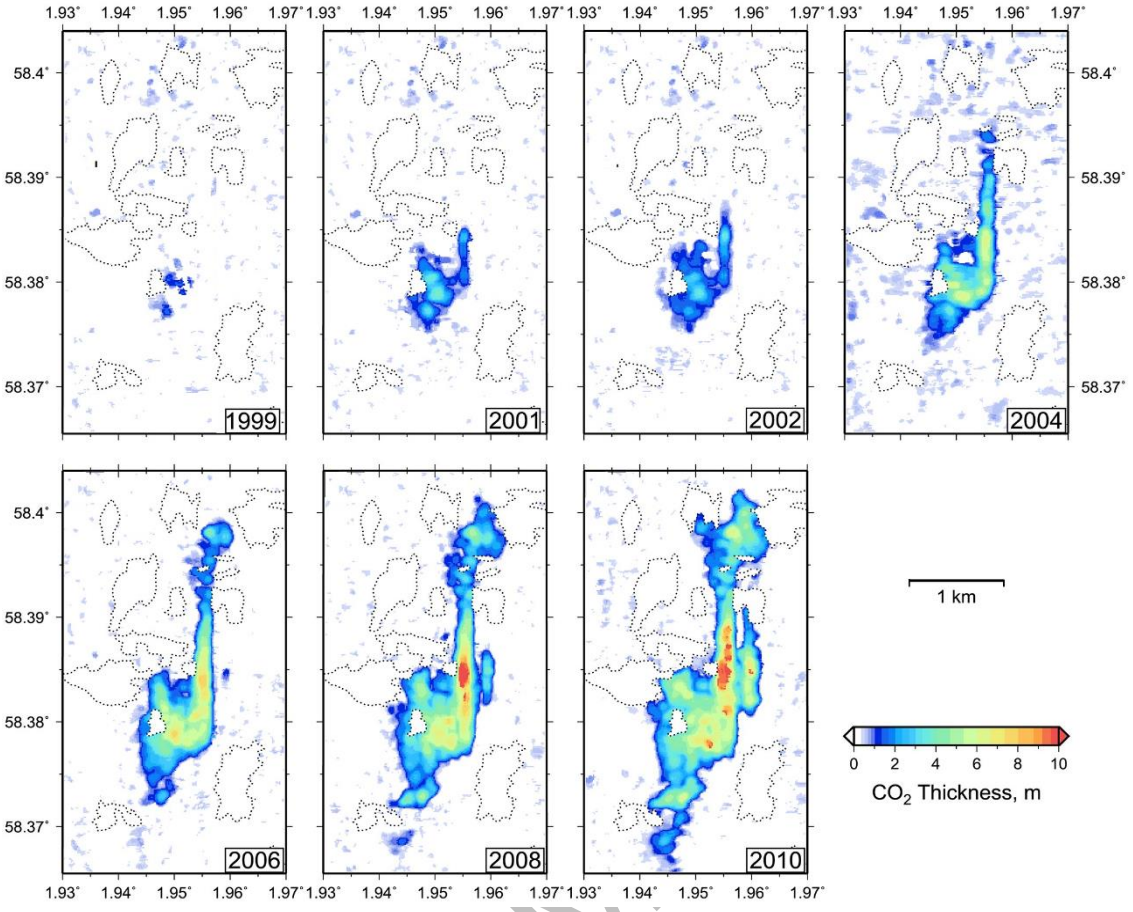

Figure 3: The mapped distribution of CO_2 in the uppermost layer beneath the caprock (Layer 9) as interpreted from 4D time-lapse seismic. [Source: Cowton et al.,[11]]

2 Problem statement

The nature of the CO_2 supply to the Utsira sand wedge and the distribution of CO_2 plume within it depend on the transport properties of Utsira mudstones and the sand wedge, respectively. Explanations for the observed growth of the CO_2 plume in the topmost layer include:

a) the unlikelihood that CO_2 migration through the mudstones is entirely governed by visco-capillary Darcy flow but rather via some form of pathway flow[12] and

b) the presence of high permeability channels, herein referred to as 'thief zones', within this layer with a preferential north-south flow direction (see Figure 4).

Suggestions on the origin of pathway flow include faulting or minor collapse induced by fluidisation within the main feeder chimney identified in Figure 2a[13] and the presence of 'holes'

in the Utsira mudstones possibly due to erosion or sand mobilisation.[7] Regardless of the origin of these pathways, the flow property of the mudstones plays a vital role in moderating the upward migration rate of the CO_2 plume.[14] For instance, the relative permeability to CO_2 in the mudstone baffles is likely to increase as they become more saturated with CO_2.[10]

The influence of channelling in the top sand wedge on the CO_2 plume migration has been investigated by Williams and Chadwick[15] and Cowton et al.'[16] through the effects of permeability heterogeneity and plume temperature. This approach yielded a better match between the observed and calculated CO_2-water contact (CWC) for most of the sand wedge but failed to match the observed migration rate of CO_2 along the prominent northern ridge.

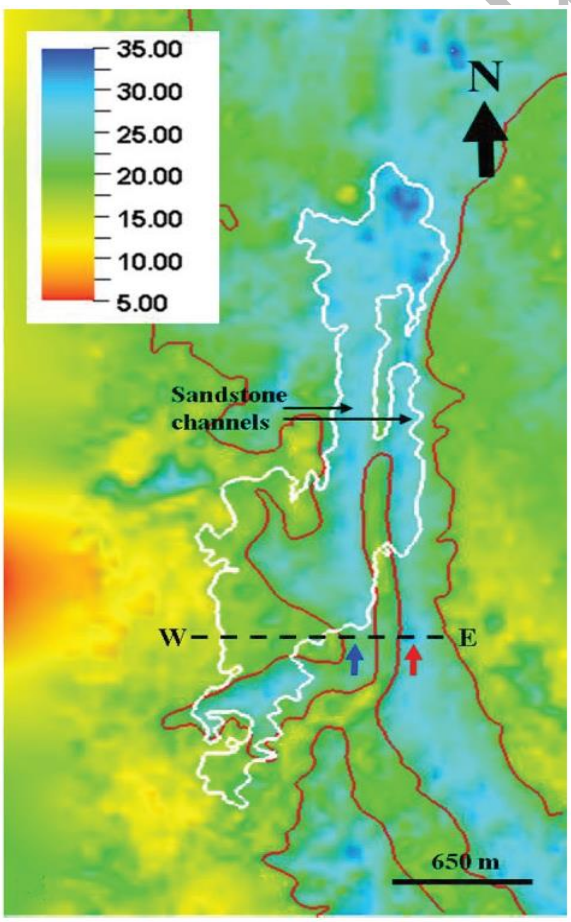

Figure 4: Shaded isochore map (ms) of the top sand-wedge from seismic mapping. Cold colours denote thicker reservoir (channels) with the blue and red arrows show individual channels. Warm colours highlight thinning in the reservoir above mud diapirs. The red polygon outlines a 20 ms isochore. The white polygon delineates the margins of the topmost CO_2 layer in 2010. The dotted line shows the location of the seismic section. [Source: Williams and Chadwick[15]]

The seismic time-lapse datasets have been applied using various simulation approaches to assess uncertainties that exist and approximate history match at the Sleipner storage formation.[14,17–19] These include the pressure performance,[20] the reactive transport in Layer 9,[21,22] and a greater emphasis on the quantification of CO_2 plume.[11,23–27] Zhu et al.'s[28] history matching of CO_2 plume migration in the Utsira Formation, through simulating sensitivity on pressure, temperature, intrinsic permeability, relative permeability curves, feeders, spill rates and methane (CH_4) content in the CO_2 stream, concluded that the CO_2 plume extent is only sensitive to permeability anisotropy, temperature and CH_4 content. However, the concept of relative permeability sensitivity was not elaborated on in the text and requires further clarification. Additionally, the lack of sensitivity to relative permeability as established in Singh et al.,[18] was based on a steady-state upscaling of $k_r - S_w$ curves using the viscous-limit assumption. Nevertheless, relative permeability functions have been shown to have a significant impact on estimations of CO_2 trapping mechanisms such as structural, residual and even solubility trapping.[29–31]

The term 'viscous-limit' is used to describe viscous-dominated displacements where fluids are transported in response to an applied external force *i.e.* the viscous force. The magnitude of the viscous force is mainly dependent on the pressure gradient and the fluid viscosities, and not the fluid and rock interactions *i.e.* capillary forces. Consequently, this study investigates the sensitivity of CO_2 plume to relative permeability based on the capillary-limit assumption. This process employs the establishment of casual relationships between the pore-size parameter and the Capillary Pressure – Relative Permeability – Wetting Saturation ($P_c - k_r - S_w$) curves described in Onoja et al.,[32] to characterise the dynamic flow state of interbedded mudstone units and high permeability sand channels in the Utsira Formation using the van Genuchten[33] empirical model. To this end, the current study is especially interested in two key performance measures:

i) How the $P_c - k_r - S_w$ functions of the intra-sand mudstones influence the maximum vertical migration distance of CO_2 from the injection point to the top of the reservoir, and

ii) How the $P_c - k_r - S_w$ functions within 'thief zones' in the sand wedge influence the plume footprint area.

The flow simulations presented in this study are based around the time-lapse seismic monitoring programme at the Sleipner Field. This is to enable the exploration of the performance measures stated above in the numerical simulation of CO_2 injection in a sandstone aquifer interbedded with laterally continuous mudstones. It is important to stress that this study does not attempt to reproduce observed fluxes of CO_2 plume derived from the seismic data but to investigate the impact of capillary-limit relative permeability curves in the interbedded mudstone and high permeability sand channels on the growth of CO_2 plume.

3 Numerical flow simulation

The flow simulations employ two modelling scenarios to review and analyse the performance measures identified in the preceding section. The first case study simulates the Darcy flow of CO_2 through saturated porous media using an axisymmetric model (Section 3.1) while the second case study investigates the temporal evolution of the topmost CO_2 layer in three-dimensions using the Sleipner Benchmark model of the topmost reservoir layer or 'sand wedge' (Section 3.2). ECLIPSE 100 'black oil simulator' is used to simulate CO_2 injection in both cases.

The default solution procedure in ECLIPSE 100 for all black oil runs is fully implicit. This generally allows for large time-steps in the simulation and uses Newton's method[34] to solve the non-linear equations. For dynamic simulations herein, the fully implicit solution option is activated to avoid convergence problems that may arise from flow reversals. This is because a fully implicit solution solves all the variables simultaneously in the linear solver, unlike the other options in ECLIPSE, i.e. IMPES (implicit pressure, explicit saturations) and AIM (adaptive implicit) methods, which may rely on some solution values from the previous time-step.[35]

In order to avoid convergence problems that may arise from phase change behaviour during simulation, the default maximum length of time-steps in the fully implicit option, i.e. 365 days, is reduced to 20 days. This limit is used to ensure time-step chopping and that the multiphase solution does not move too quickly through a grid block because the front between the two phases may not be actually tracked through that block. Additionally, the maximum number of Newton iterations is increased from the default value of 25 to 60. These are implemented by activating the TUNING option in the SCHEDULE section and adjusting the time-stepping and iteration controls.[36] NB: Time-step chopping is what happens when the solution does not converge within the maximum number of non-linear iterations. In that case the time-step is chopped – its size is reduced tenfold – and the step is repeated to see if convergence can then be obtained.[35]

Finally, a control is included in the simulation data to stop running following any time-step convergence failure. This is done by activating and tuning the 27th item in the OPTIONS keyword within the SCHEDULE section of the data-file.[36]

3.1 First Case Study

A radial axisymmetric mesh that incorporates the properties of the Utsira Formation is used to simulate the growth of CO_2 plume. The model is kept relatively simple to allow multiple model scenarios to be run within a reasonable computation time. The outer boundary of the model is set at radius of 6 km to accommodate the lateral spread of the CO_2 plume during the injection period. Horizontally, cell dimensions start at 2.5 m at the axis expanding to 5 m between radial distances of 100 m and 200 m, 10 m between 200 m and 400 m, 20 m between 400 m and 800 m, 30 m between 800 m and 1500 m with further expansion thereafter reaching 50 m at the outer boundary. The modelled reservoir domain is 220 m thick and contains seven thin mudstones which should allow up to eight spreading layers of CO_2. The vertical spacing of the mudstones match the estimated spacing between the mapped reflections[37] and are described in Figure 5.

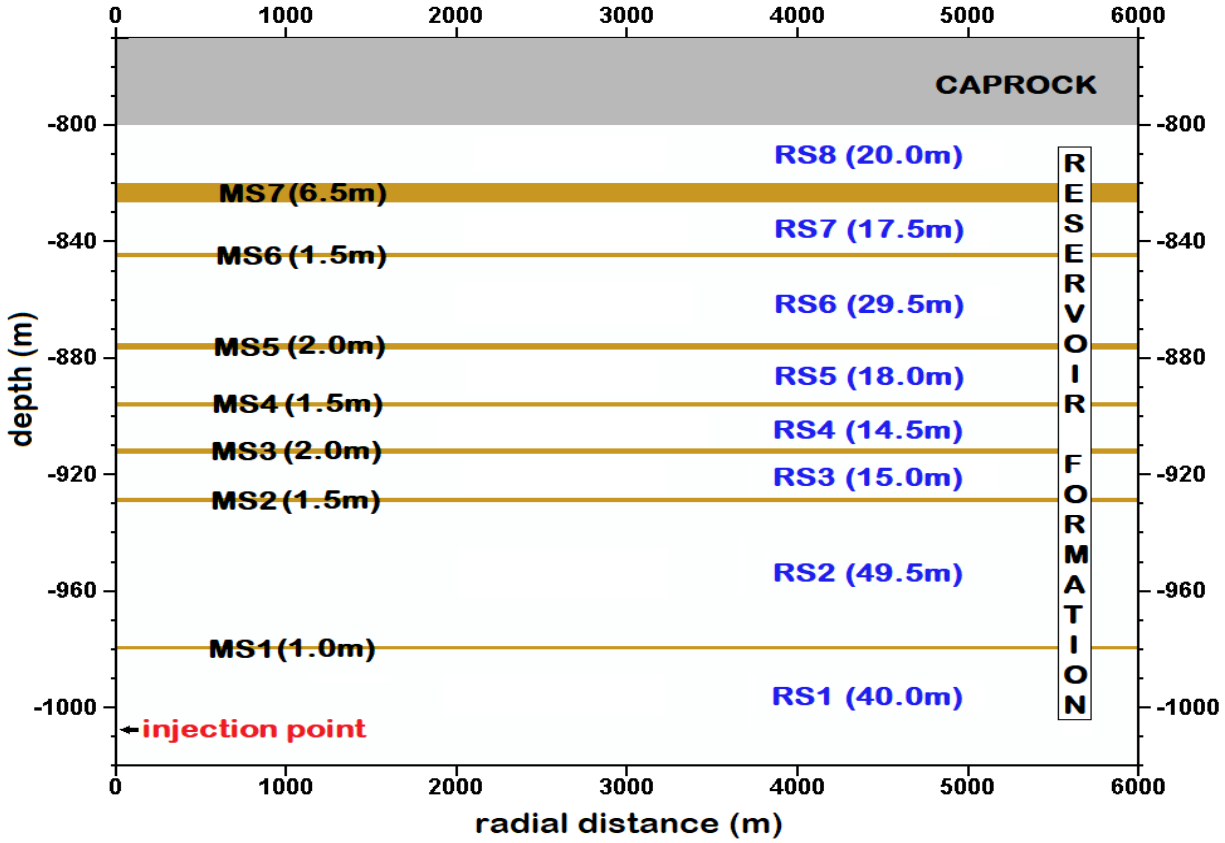

Figure 5: Schematic description of the model geometry in the r-z cross section showing the reservoir zones [RS1 – RS8] and the interbedded mudstone layers [MS1 – MS7] as well as their thicknesses in bracket. Not to scale.

P_c – k_r – S_w relations (Figure 6) are computed using the van Genuchten function illustrated in equations 1 – 4 below:

$$S_{ew} = \frac{S_w - S_{wr}}{1 - S_{wr}} \tag{1}$$

$$S_{ew} = \left[1 + \left(\frac{P_c}{P_e}\right)^n\right]^{-m} \tag{2}$$

$$k_{rw} = (S_{ew})^{0.5}\left[1 - \left(1 - (S_{ew})^{1/m}\right)^m\right]^2 \tag{3}$$

$$k_{rn} = k_o * [(1 - S_{ew})^2 * (1 - S_{ew}^2)] \tag{4}$$

where S_{ew} is the effective wetting phase saturation, S_w is the wetting saturation, S_{wr} is the residual wetting saturation, P_c is the capillary pressure, m and n are pore geometry parameters related by the assumption that $m = 1 - 1/n$, P_e is the capillary entry pressure, k_{rw} is the relative permeability

to brine, k_{rn} is the relative permeability to CO_2, and k_o is the maximum relative permeability value for the nonwetting phase. NB: The van Genuchten empirical model described in equations 1 – 4 describes a $P_c - k_r - S_w$ relationship that is more applicable to a wider variety of sediments.[38] This model results from the coupling of van Genuchten's[33] analytical and Mualem's[39] geometrical formula to describe capillary pressure and relative permeability functions during fluid flow through porous media. The Mualem formula can only be integrated analytically to the van Genuchten formula if $m = 1 - 1/n$.

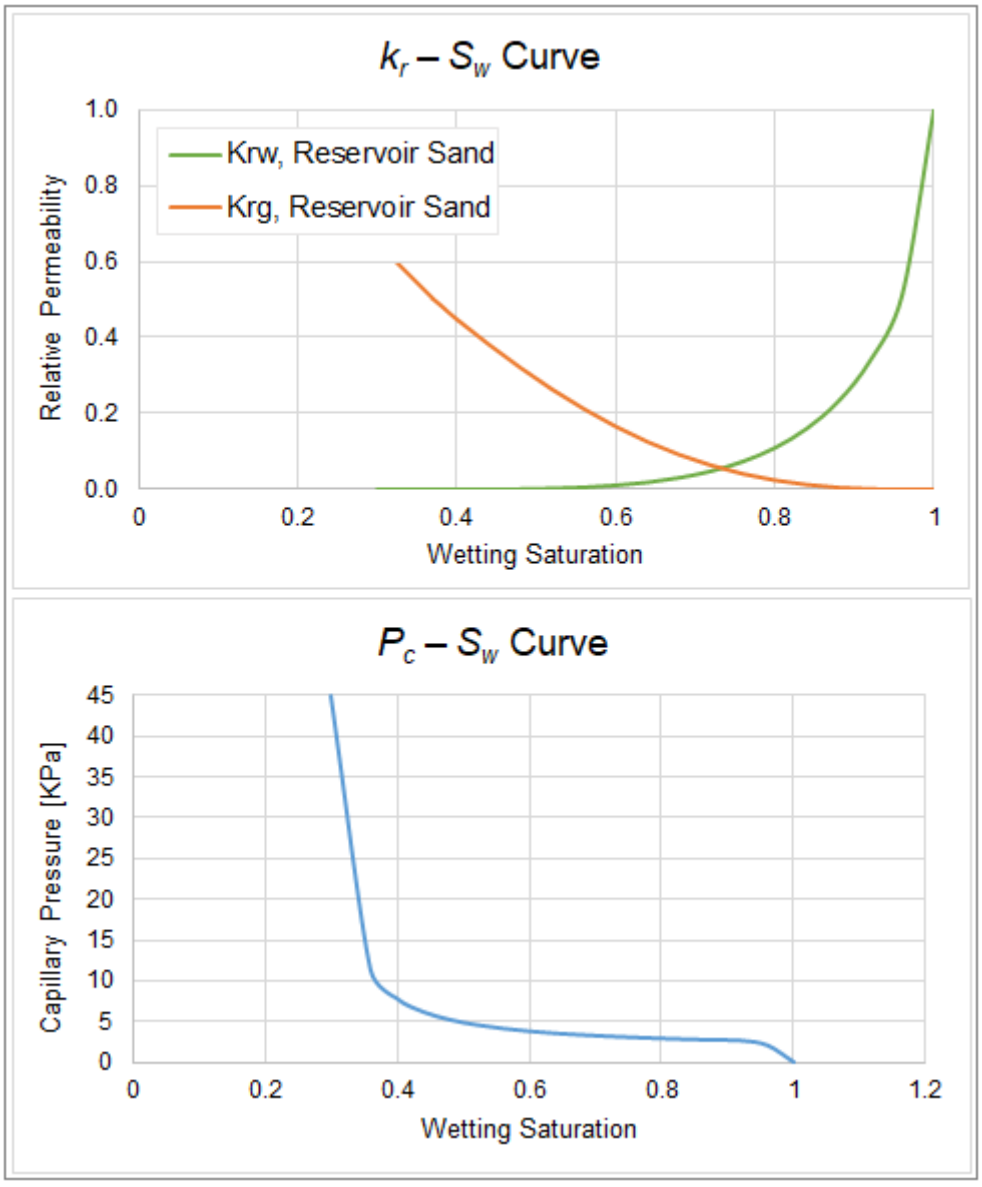

Figure 6: $P_c - k_r - S_w$ relationship for the reservoir sand

Assumptions for the reservoir sand include an average permeability and porosity of 2000 mD and 0.36, respectively.[18] $P_c - k_r - S_w$ relations based on a capillary entry pressure [P_e] of 0.00172 MPa (which correlates experimental values for the Utsira sand)[40], an arbitrary residual wetting saturation [S_{wr}] of 0.3, and a pore geometry parameter [m] of 0.56 for clastic sandstone.[32]

In the modelled domain a single vertical injection well is located at $r = 0$ with CO_2 injection at an annual rate of 1 million tonnes for twenty years. The injection rate applied herein is based on the average injection rate at the onset of CO_2 injection in the Sleipner Field.[8] Two flow scenarios are modelled in the numerical flow simulation. At the outset, CO_2 migration through the mudstones is inferred to occur by viscous-dominated Darcy flow along discrete pathways. These pathways are assumed to originate at $r = 0$ of each intra-sand mudstones with a constant aperture of 2.5 m. This was adopted as the only position for holes in the thin shale layers since previous research by Cavanagh and Haszeldine[17] confirmed that the CO_2 stacked layers are insensitive to variations in the precise position of holes in the shale layers. It is noted that the viscous force usually dominates the displacement process at the field scale and its magnitude is dependent on the applied pressure gradient (*i.e.* externally applied force) and the fluid viscosities.[41] The second scenario assumes CO_2 migration through the mudstones is strictly by capillary-dominated Darcy flow. Capillary forces dominate the displacement process in the pore scale. Breakthrough pressures and $P_c - S_w$ curves for porous media manifest the capillary forces at the interface between CO_2 and brine in the pore throats of the porous media. The sensitivity analysis of both scenarios is expected to provide insights into the buoyant migration of supercritical CO_2 across low permeability mudstone baffles and barriers within a sandstone reservoir.

3.1.1 Pathway flow analysis

Initial flow properties of the mudstones are based upon a capillary entry pressure of 1.72 MPa for the Nordland Shale.[12] The permeability of intra-sand mudstones are considered to be ultra-low with an intrinsic permeability value of 0.001 mD and a porosity of 0.35, after the Nordland Group

caprock. The $P_c - k_r - S_w$ function of the thin mudstones is computed using a pore geometry parameter [m] of 0.29 and a residual wetting saturation [S_w] of 0.605. Pathways in the interbedded mudstones are represented by either increased permeability values, $P_c - k_r - S_w$ functions for the reservoir sand, or both in some cases.

Flow simulation indicates that the injected supercritical CO_2 ($scCO_2$) ascends due to the gravity segregation resulting from the density contrast between the invading gas and *in situ* brine. The flow properties of each reservoir are constant with an average permeability of 2000 mD, which implies that capillary forces within the sand units are not an issue for the mobility of the plume. However, in the presence of intra-sand argillite units, as is the case here, if the capillary pressure [P_c] of the invading fluid does not exceed the entry pressure of the thin mudstone layer, the fluid will pond beneath the capillary barrier, migrating laterally along its topography until a spill-point or an opening for vertical migration is reached. The assumption of vertically aligned pathways in the mudstone layers invariably serves as a conduit for viscous-driven Darcy flow to produce a multi-layered CO_2 plume in the reservoir formation.[42,43] In the first instance, the sensitivity cases described in Table 1 highlights the sensitivity of the CO_2 plume contact area to the flow properties of these pathways. A qualitative insight into the plume dynamics is provided through two distinctive elements: the vertical migration of the plume, where the mobility of the gas through each sand layer is mainly a function of the pathway's flow properties, and the amount of free gas (mobile and immobile) within layers of reservoir sand at the end of simulation.

In Figure 7, a comparison of the sensitivity cases in pairs, *i.e.* P0 vs P1, P2 vs P3, and P4 vs P5, support the proposition that the relative permeability functions could serve to enhance or retard the mobility of non-wetting fluid through the aperture. This is irrespective of the presence or absence of capillary forces in the pathway. Although pathways modelled by the intrinsic permeability value alone promote the development of a multi-layer plume, the inclusion of the relative permeability curve for a less compact lithology improves the mobility of gas through the

aperture. This serves to increase the quantity of CO_2 in each overlying layer and shows that the relative permeability function of the pathway in the thin argillite layers, especially the first argillaceous layer, is fundamental to fluid flow through the reservoir. This is highlighted in Figure 8 where cases P0 and P3, modelled with the same effective permeability for pathway flow, show the ease of gravity drainage from RS1 into overlying reservoir zones: RS2, RS3 and RS8. The sensitivity of pathway flow to capillary forces and relative permeability is emphasised in Figure 7c. In this illustration for cases P4 and P5, the mudstones act as impermeable barriers that lead to the accumulation of a single layer of CO_2 beneath the first mudstone (MS1) in the reservoir formation.

The presence of pathway flow in P4, modelled via $P_c - k_r - S_w$ functions of the reservoir sand where the capillary entry pressure is 1.72 KPa, allows the buoyant migration of CO_2 through the first mudstone layer (MS1) into the overlying sand layer, unlike case P5 (see Figure 8b). This identifies two main hypotheses:

i) The capillary forces acting in a porous media can significantly impede the rate of CO_2 migration through it; and

ii) At an intrinsic permeability value of 0.001 mD and a capillary entry pressure of 1.72 MPa, the relative permeability distribution along a 1m-thick laterally extensive argillite layer becomes an important feature for assessing fluid migration through the flow barrier.

In the absence of capillary forces, as seen in cases P2 and P3, the pathway flow becomes a function of the effective permeability of the aperture. Figure 8d further illustrates the relevance of relative permeability functions in the transport properties of the aperture when comparing cases P2 and P3. The sandstone $k_r - S_w$ curves modelled into the vertically aligned pathways in case P3 resulted in the increase of CO_2 volume flow to the top of the reservoir *i.e.* RS8.

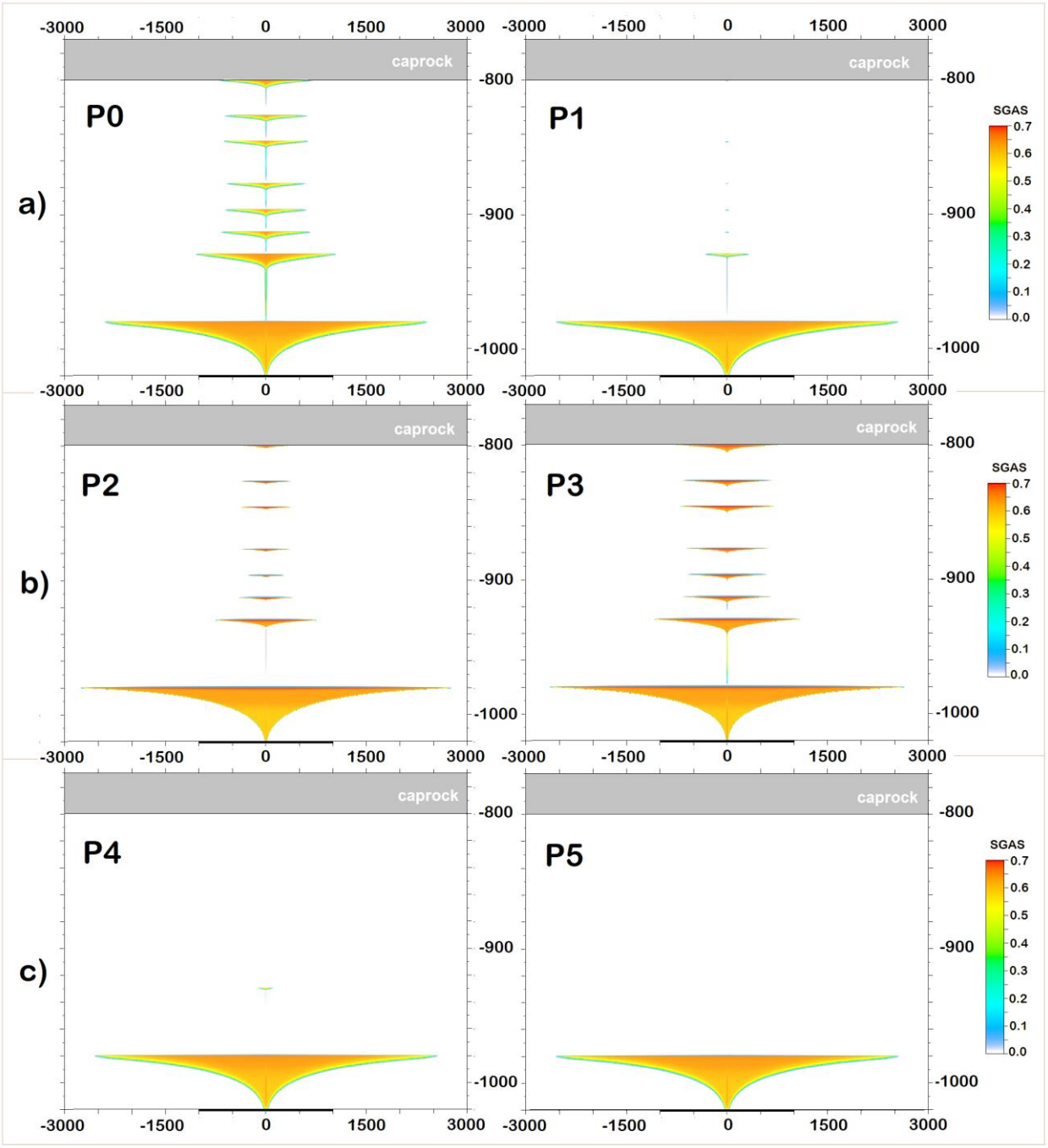

Figure 7: Comparison of CO_2 plume distribution at the end of simulation for cases a) P0 & P1, b) P2 & P3, and c) P4 & P5. NB: Depth and distance in metres (m)

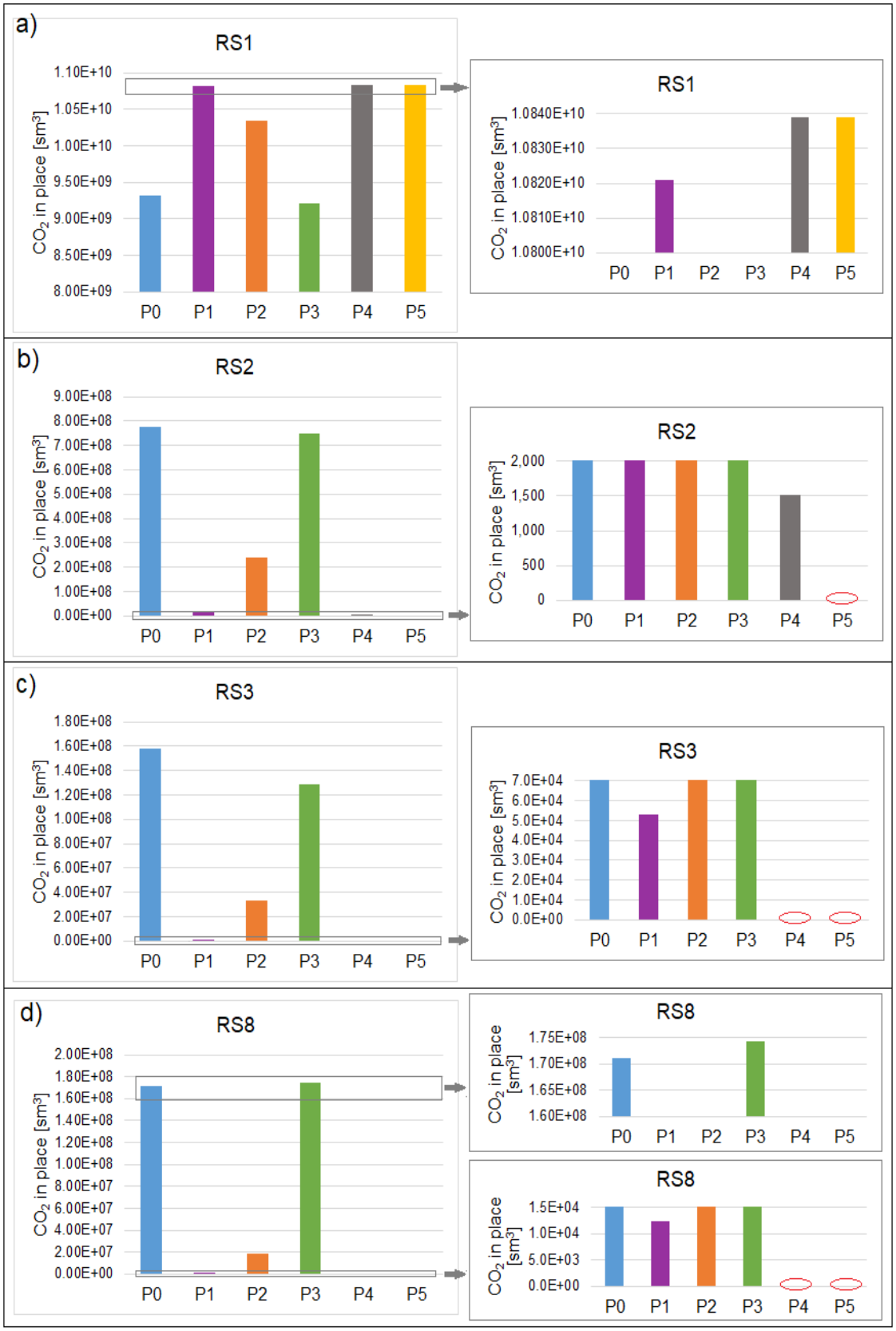

Figure 8: Volume of CO_2 in place in reservoir zones a) 1, b) 2, c) 3 and d) 8 at the end of simulation. NB: Red circles in 8c & d depict zero CO_2 accumulation in the respective case.

3.1.2 Capillary flow analysis

In this section, CO_2 migration through the intra-sand mudstones is assumed to occur by capillary-limit flow. The permeability and capillary entry pressure of the intra-sand mudstones play a key role in moderating the rate of upward migration of CO_2 through the reservoir. These properties are adjusted so that the flow simulation matches the arrival of CO_2 at the top of the reservoir in the third year of injection, as detected by the time-lapse seismic monitoring programme at Sleipner site.[8] The assumed permeability of the mudstones for this analysis was empirically derived under viscosity-dominated Darcy flow where the mudstone layers are modelled without P_c – S_w functions, *i.e.* the absence of capillary forces. The resulting permeability value of 30 mD employed in the sensitivity analysis of Darcy flow physics is based on the observation of plume migration to the top unit of the reservoir (RS8) in the third year of CO_2 injection (Figure 9).

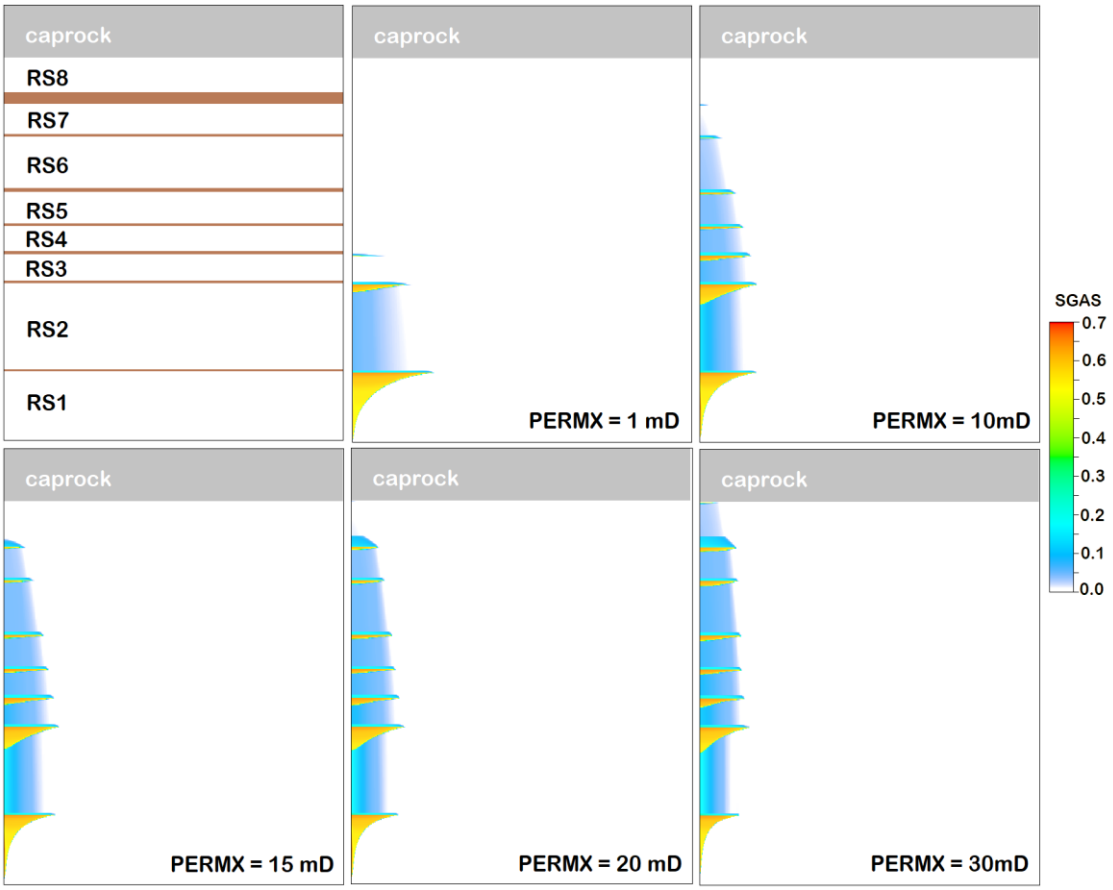

Figure 9: Multi-layered CO_2 plume migration for viscosity-dominated flow through reservoir argillite units with varying permeabilities. NB: PERMZ = PERMX x 0.1

It is worth noting that the plume morphology at the Sleipner site indicates that column heights of trapped CO_2 plume are low and a capillary entry pressure of 1.72 MPa may not be applicable to the Utsira mudstones.[17] To this end, a capillary entry pressure value three orders of magnitude less than 1.72 MPa was used for the thin argillite layers. This value was chosen by iteration to match the arrival time of CO_2 at the top of a reservoir formation in the third year of CO_2 injection when the interbedded mudstones are assigned a permeability of 30 mD. Note that the assigned permeability value is a direct consequence of the analysis described in the preceding paragraph. Figure 10 supports the hypothesis that the buoyant movement of the non-wetting phase is strongly influenced by the capillary forces in the intra-sand mudstone units. In instances where the P_c of the CO_2 plume exceeds the mudstone entry pressure, the plume breaches the mudstone layer and migrates vertically until another capillary barrier is reached. The essential feature is that the total driving force for invading fluid flow is just about adequate to overcome the semi-permeable mudstone resistance afforded by a capillary entry pressure of 1.72 KPa. Cavanagh and Haszeldine[17] attribute the possibility of such uncharacteristically low threshold pressures to the occurrence of micron-thick fractures in the mudstones. The Darcy flow model in Figure 10d portrays the pattern of pooling, breaching and vertical migration of CO_2, which matches the observed plume distribution in Sleipner. This model is identified as the base case, designated as S0, for an analysis on the sensitivity of buoyant plume migration to $P_c - k_r - S_w$ functions in the thin mudstones. Other sensitivity cases are for various argillaceous units defined in Table 2 are shown in Table 3, while Figure 11 illustrates the descriptive $P_c - k_r - S_w$ curves applied herein.

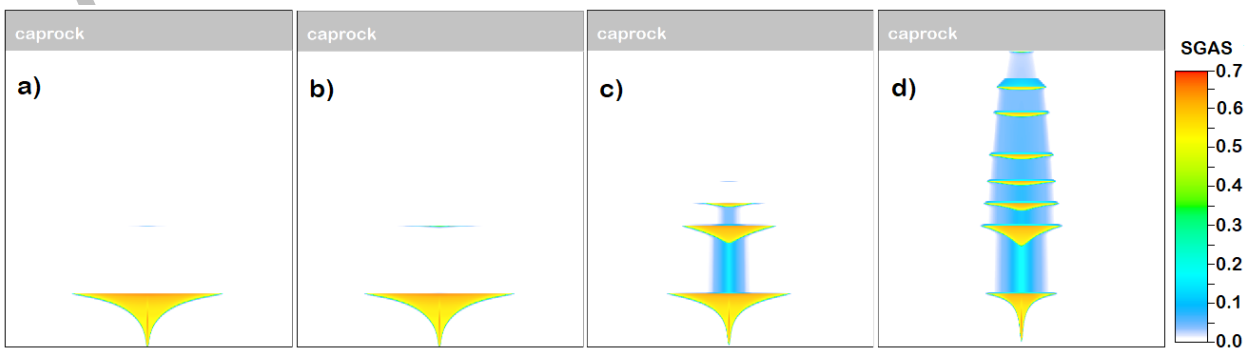

Figure 10: Buoyant migration of scCO$_2$ through intra-sand mudstone units modelled with capillary entry pressure of a) 1720 KPa, b) 172 KPa, c) 17.2 KPa and d) 1.72 KPa

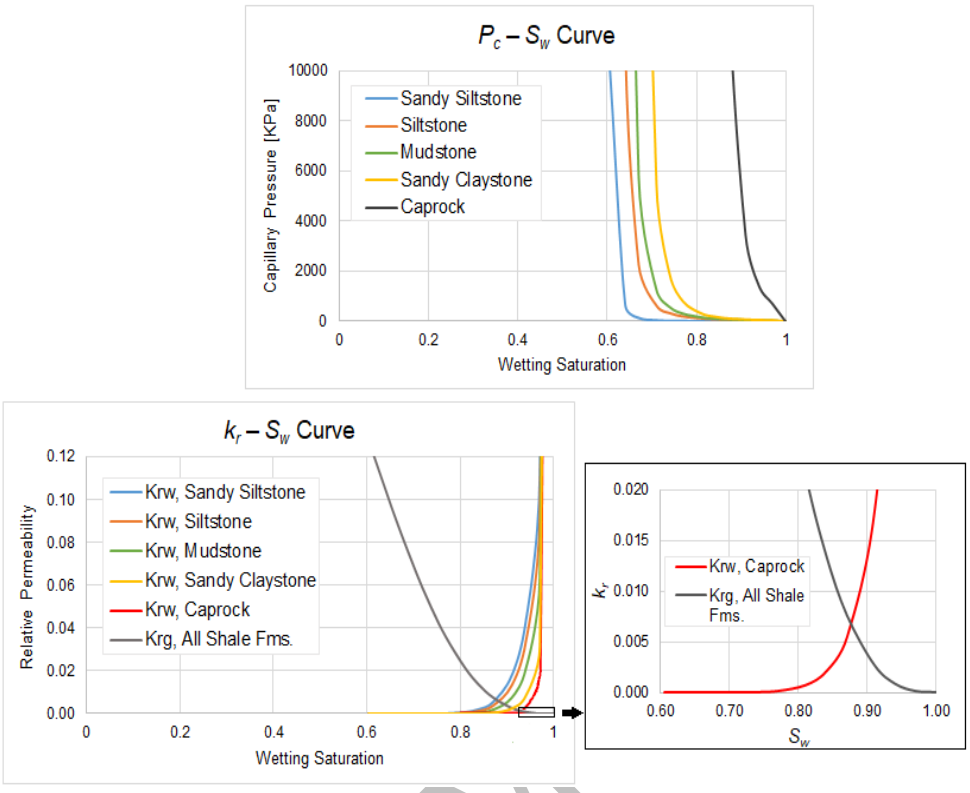

Figure 11: $P_c - k_r - S_w$ relationship for the various argillaceous units.

As CO$_2$ injection proceeds, the gas propagates under gravity along the horizontal semi-permeable argillaceous layers. Results of a 20-year injection period show that the volume of CO$_2$ plume pooling beneath the capillary barrier is essentially dependent on the transport properties of the semi-permeable strata above it (Figure 12). Sandy siltstone, which provides the least resistance to buoyant CO$_2$ migration, results in a higher degree of gas percolation through the sand enriched argillite, as opposed to the siltstone and mudstone. This is evident in the plume saturation profile in RS1 and RS2, *i.e.* Figure 12 a & c, where the thin argillite layers in cases S0, S1 and S2 are modelled as sandy siltstone, siltstone and mudstone, respectively, using the transport properties curve map in Figure 11. With a constant injection rate and an equivalent volume of CO$_2$ injected in all three cases, the loss of CO$_2$ plume in RS1 results in a higher concentration of mass at the front end of plume evolution in RS2. This gives a greater chance for the gravity current to advance through the overlying argillite layers. However, the likelihood of such occurrence is entirely

dependent on the magnitude of capillary force in the overlying argillite layer that counteracts the buoyant force in the migrating plume. Such equilibrium between the capillary force and the buoyant force is described by the Young-Laplace equation.[44] This equation relates the gravitational column height of buoyant fluid to the capillarity of the porous media using the expression below:

$$\Delta\rho gh = \frac{2\sigma\ cos\,\theta}{R} \tag{5}$$

where $\Delta\rho gh$ is quantified as the buoyancy force counteracted by the capillary force, P_c. $\Delta\rho$ is described as the density contrast between the wetting and non-wetting fluid, g is the gravitational constant, h is the column height of buoyant plume, σ is the interfacial tension between the fluid phases, Θ is the wetting angle, and R is the pore throat radius.

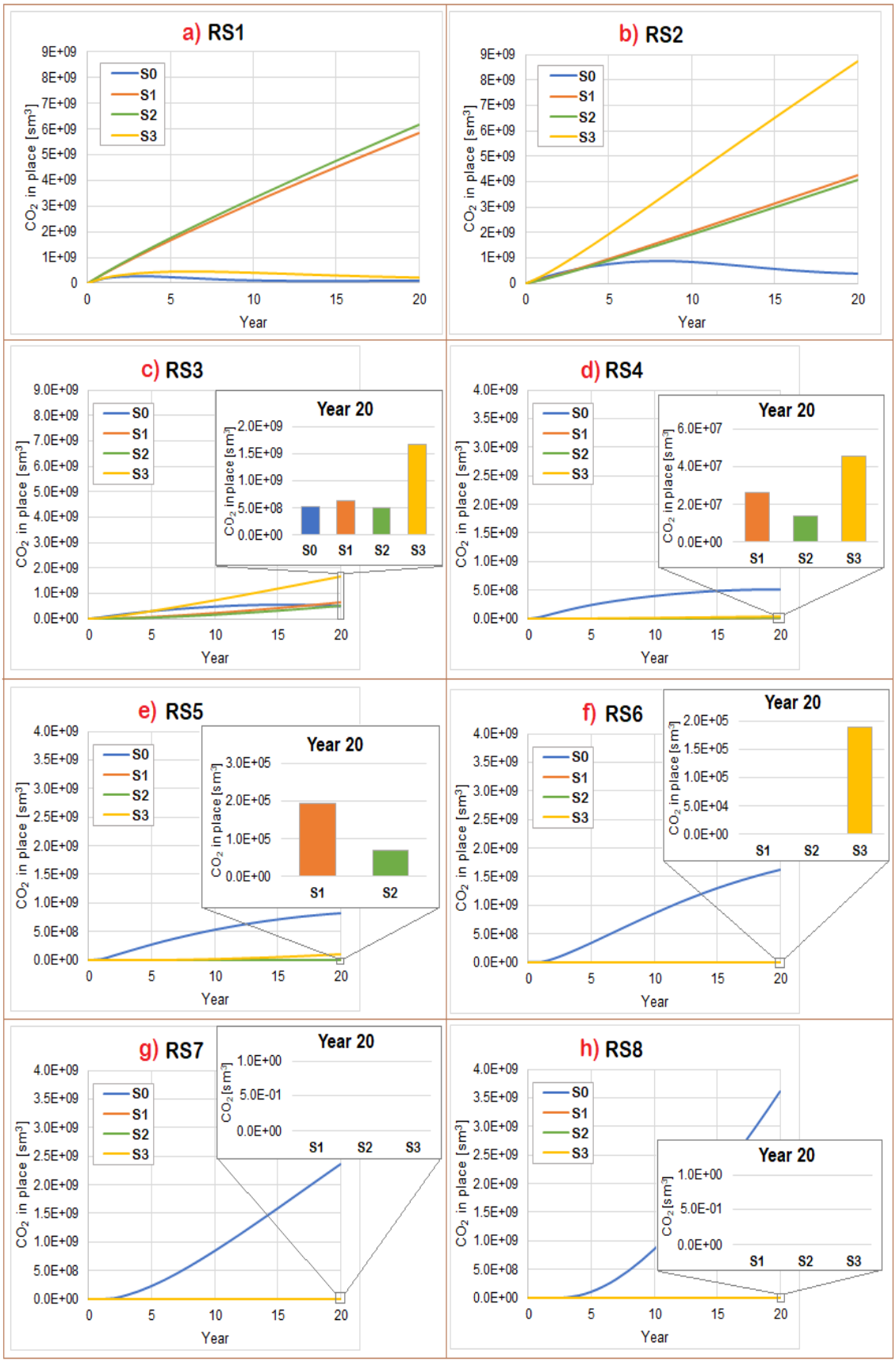

Figure 12: Profile of CO_2 emplaced during the injection period in a) RS1, b) RS2, as well as the volume of CO_2 emplaced at the end of injection in c) RS3, d) RS4, e) RS5, f) RS6, g) RS7, and h) RS8

As injection proceeds in cases S0, S1 and S2, pathways emerge for CO_2 percolation through the thin argillite layers. These pathways are a function of CO_2 breakthrough pressure and the column height of plume beneath each argillaceous layer. At a constant CO_2 pressure in the reservoir, the CO_2 breakthrough pressure for each argillaceous unit varies according the resistant force acting within the argillite layer. The mass of gravity current that then advances through each argillaceous unit is attributed to the column height of plume beneath that argillite layer. Hence, the case modelled with the least resistant force in each argillaceous unit, *i.e.* S0, show preferential migration of the plume to the top of the formation, *i.e.* RS8 (Figure 12d). This is due to the greater magnitude of buoyant force acting, with respect to the resistant force, at the top of each underlying reservoir unit, in contrast to cases S1 and S2. Case S3 elaborates on this theory where the volume profile of CO_2 plume that migrates through the first argillite (MS1) is akin to that of case S0 (Figure 12a). This is because the capillary forces acting within MS1 is the same in both cases. As the buoyant plume migrates through MS2, a divergence in the volume profile for cases S0 and S3 is evident and sets in due to the greater ease of CO_2 percolation to the overlying sand unit in the former (Figure 12c). Eventually, the varying capillary forces acting within the overlying argillite layers in case S3, which create a higher resistance to buoyant plume migration than the ones in case S0, results in shorter vertical migration through the reservoir formation (Figure 12d). This shows that the number of layered CO_2 plumes resulting from horizontally persistent thin argillite units in a homogeneous sandstone is highly dependent on the capillary force acting within each unit. The main feature captured by the modelled cases is the impact of the relative permeability and capillary pressure curves on the buoyant drainage of CO_2 through the thin argillite layers. The introduction of variance in capillary pressure curves at the same capillary entry pressure gives rise to local scale capillary forces that may lead to partially saturated currents of CO_2 in the pore matrix of the argillaceous layer. Likewise, varying the relative permeability curves also affects the effective permeability of the intra-sand argillite layers. Thus, the rate of plume advancement is dependent,

not just on the capillary entry pressure, but also on the correlated structure of the rock fabric's local capillary curve and the relative permeability to the invading fluid.

3.2 Second Case Study

Judging from the plume migration trend at Sleipner, where CO_2 plume reaches the top layer by the third year of the CO_2 injection and steadily increases through the ensuing years of injection (see Figure 3), it seems most of the injected CO_2 will accumulate at the top layer in the longer term. Hence, the sensitivity of the topmost accumulation to high permeability channels or thief zones within the sand wedge should prove to be a pointer for the longer-term behaviour of the plume. This is done using the benchmark model constructed for Sleipner's uppermost sand wedge, commonly referred to as the Sleipner Layer 9 Benchmark Model, which has a grid resolution of 50 m in the XY direction and 1 m in the Z direction (Figure 13).

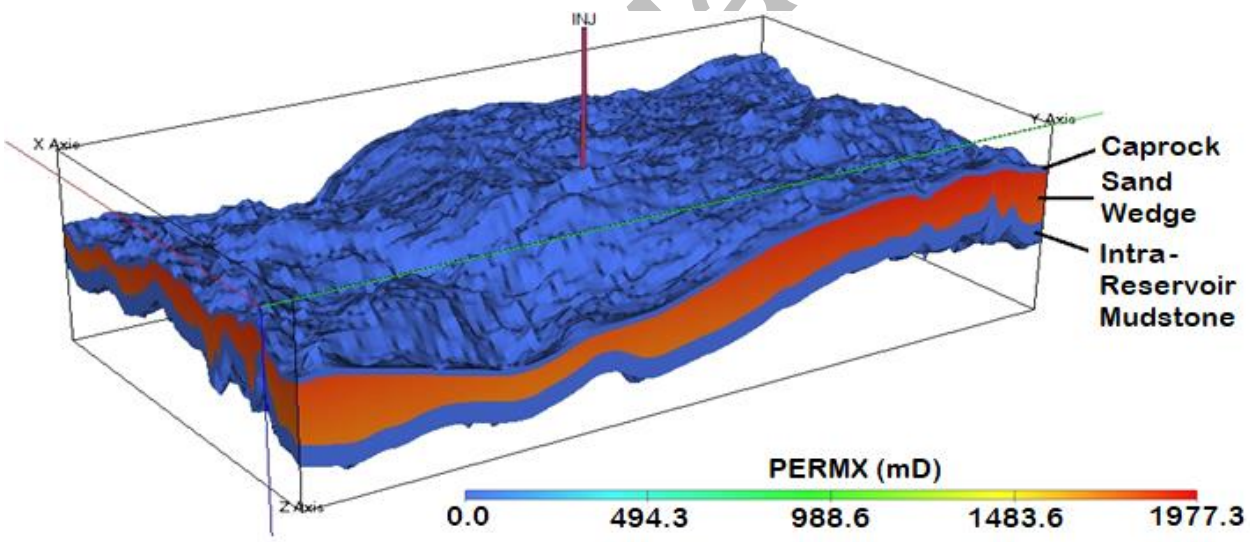

Figure 13: Sleipner Layer 9 Benchmark Model showing estimated horizontal permeability.

Singh et al.,[18] defined input parameters derived from best estimates to provide an accurate rock and fluid property dataset for the model, including the anticipated injection rate in the sand wedge that replicates the volume profile of CO_2 within it. Refer to Appendix A of Singh et al.,[18] for the benchmark model assumptions and input parameters. This study employs relative permeability functions to describe thief zones within the sand wedge. It differs from Williams and Chadwick's[15]

approach which uses absolute permeability to describe the thief zones. The base case for the sensitivity study in this section uses the laboratory-measured $k_r - S_w$ curve obtained from Singh et al.,[18]. This is fitted to the van Genuchen model using the parameters in Table 4. Cases for analysing the influence of channelling in the top sand wedge on the CO_2 plume migration through the effects of relative permeability heterogeneity are defined in Table 5.

Different relative permeability curves are computed using varying pore geometry values in Table 5 while keeping the end-point of relative permeability to the immiscible fluids and their saturation values constant. Laboratory-measured P_c data for Utsira Sand[40] is used and held constant for all the sensitivity cases. CO_2 injection is simulated in the Benchmark model for 11 years to replicate the distribution of CO_2 in the upper layer from 1999 to 2009 using Singh et al.'s[18] injection rate assumptions. Figure 14 shows the capillary pressure and injection profile used in the study, as well as the regions for channelling in the benchmark model. The northerly and southerly channels are modelled into the top half of the reservoir column to accommodate CO_2 gravity currents that are expected to spread radially from the injection point. This is because a common feature of Darcy flow simulations for CO_2 injection in a homogeneous saline formation is the predictable coning of CO_2 plume away from the injection location.[45]

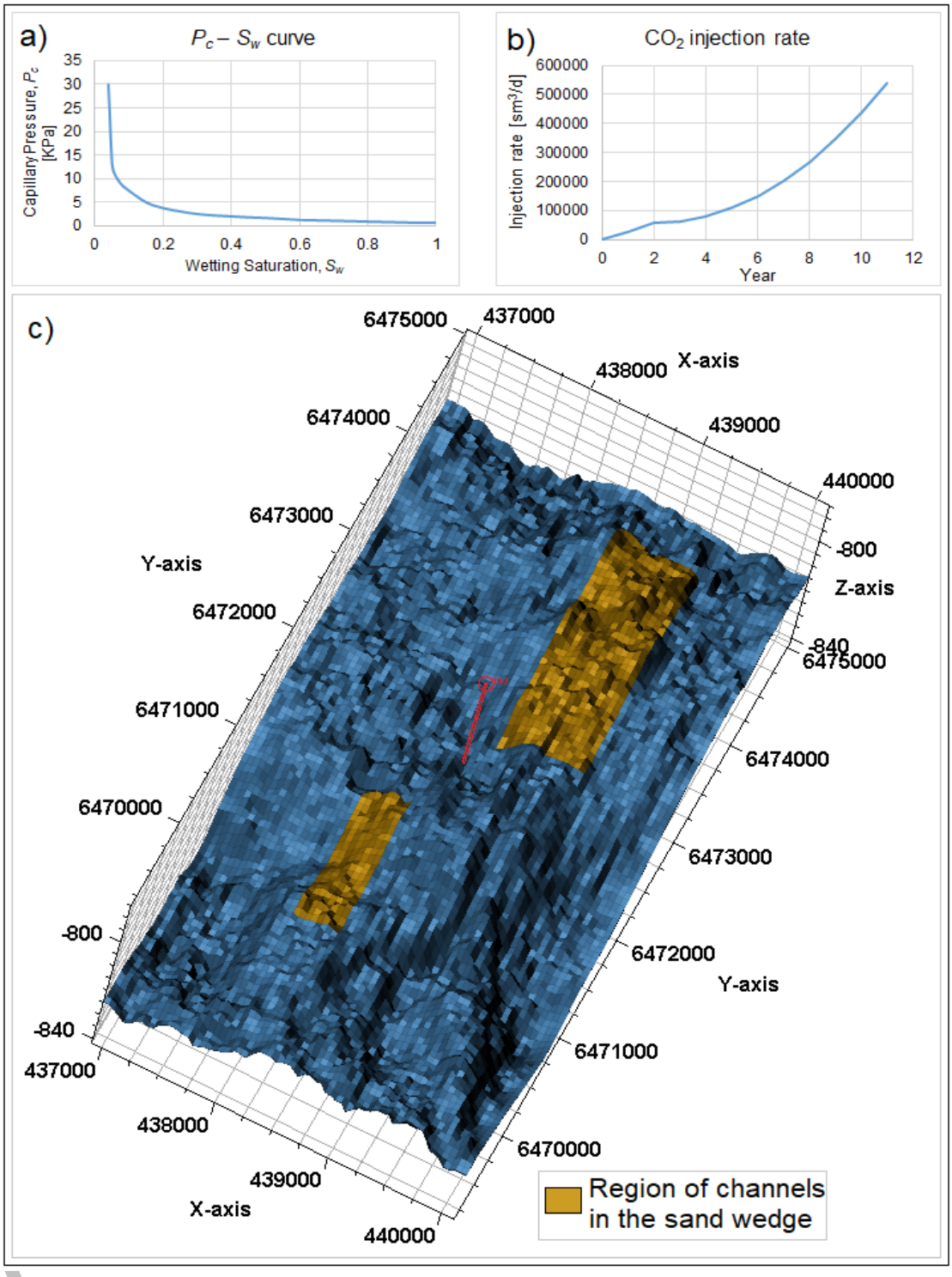

Figure 14: Illustration of the a) capillary pressure curve for Utsira Sand, b) the injection profile, and c) the regions for channelling in the Sleipner Layer 9 Benchmark Model.

3.2.1 Pressure-driven analysis

Figure 15 illustrates the CO_2-water contact observed in the top layer of the sand wedge at the end of the simulation run. None of the simulation outcome displayed the observed morphology of CO_2 plume at the top of the sand wedge in the seismic data set (Figure 15). Cavanagh[46] has shown that

a long period for pressure compensation post CO_2 injection would allow black oil simulation to attain equilibrium, thus improving the plume distribution when calibrating flow simulations to the time-lapse seismic observations. Moreover, successful numerical attempts at yielding a close match in the observed CO_2 plume morphology were through simulated sensitivity on the number of feeder wells,[46] and the methane content in the CO_2 stream,[28] the permeability anisotropy,[10,37] and the plume temperature.[15] Regardless, none of these parameters was included in this flow model because the history matching of the plume morphology in the sand wedge is not within the scope of this study.

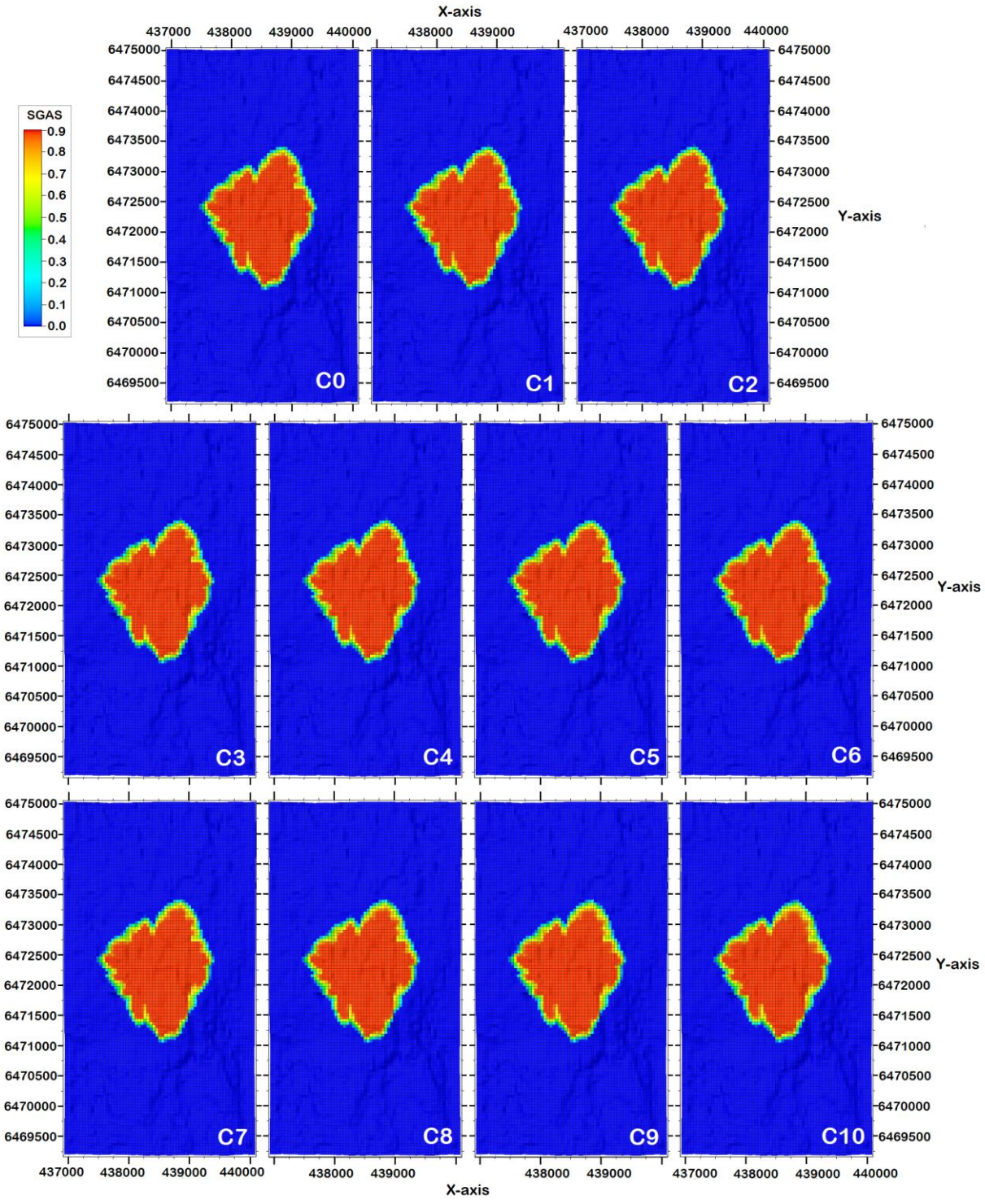

Figure 15: CO_2 plume morphology in the top layer of the sand wedge at the end of simulation

At first glance, Figure 15 showed identical morphology in the northerly and southerly plume extensions for all cases. However, on closer inspection of the grid blocks (at an expanded scale of 500%) the comparable area of plume extension only applied to the following cases: C0, C1, C2, C3, & C4; C5 & C6; C7 & C8; and C9 & C10. This could be attributed to the values of *m* for the

cases in each grouping, where *m* becomes equivalent when it is rounded up to one decimal place (see Table 5). As a result, the effect of the relative permeability curve on fluid flow is negligible. Building on this narrative, cases C0, C6, C8 and C10 were selected as representative cases for each grouping to further examine the plume extension in the northerly and southerly channels (Figure 16). Recall that the simulation resolution of each grid block is 50 x 50 x 1 m.

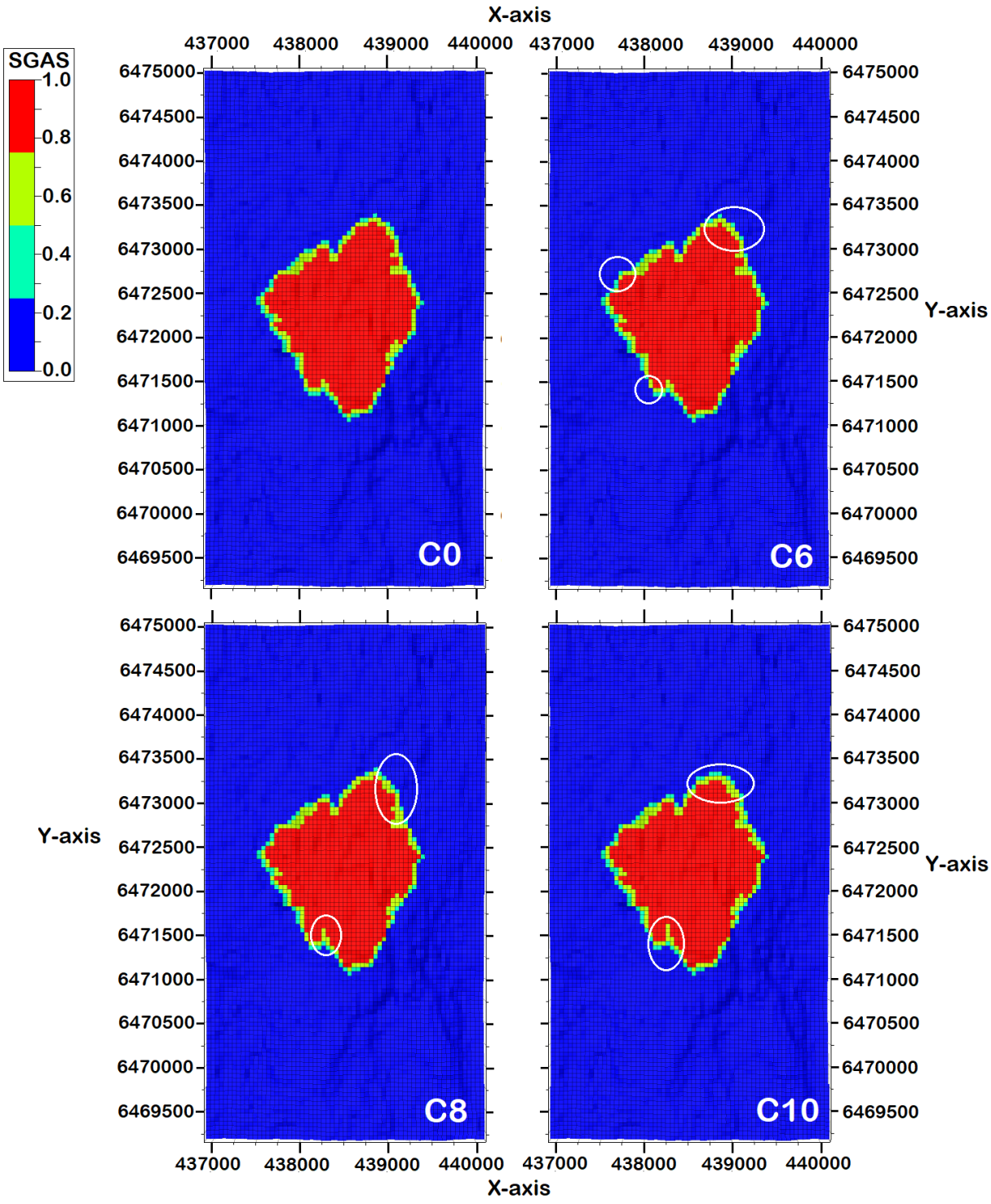

Figure 16: CO_2 plume morphology in the top layer of the sand wedge for the representative cases. NB: The white circles on C6, C8 and C10 are used to highlight the regions of plume shortening in comparison to the base case, C0.

In Figure 16, Case C0 was found to show the largest plume extension while C10 showed the least. This is readily attributed to the value of *m*, where higher values would portray a higher relative permeability to CO_2. The volume of CO_2 that migrated to the northerly and southerly channels was

quantified and illustrated in Figure 17 for the four cases: C0, C6, C8, and C10. The mass of CO_2 in the both the norther region [NR] and the souther region [SR] was largest for C0 and followed a downward trend for case C1 through to C10. This would suggest that the chanelling of gravity currents at the top of the reservoir is sensitive to relative permeability functions, however insignificant it may seem. The inclusion of heterogeneity in the capillary pressure functions could further highlight the sensitivity at this scale. These functions have already been shown to be essential in assessing the rate of CO_2 leakage seepage in pathway flow (Section 3.1.1).

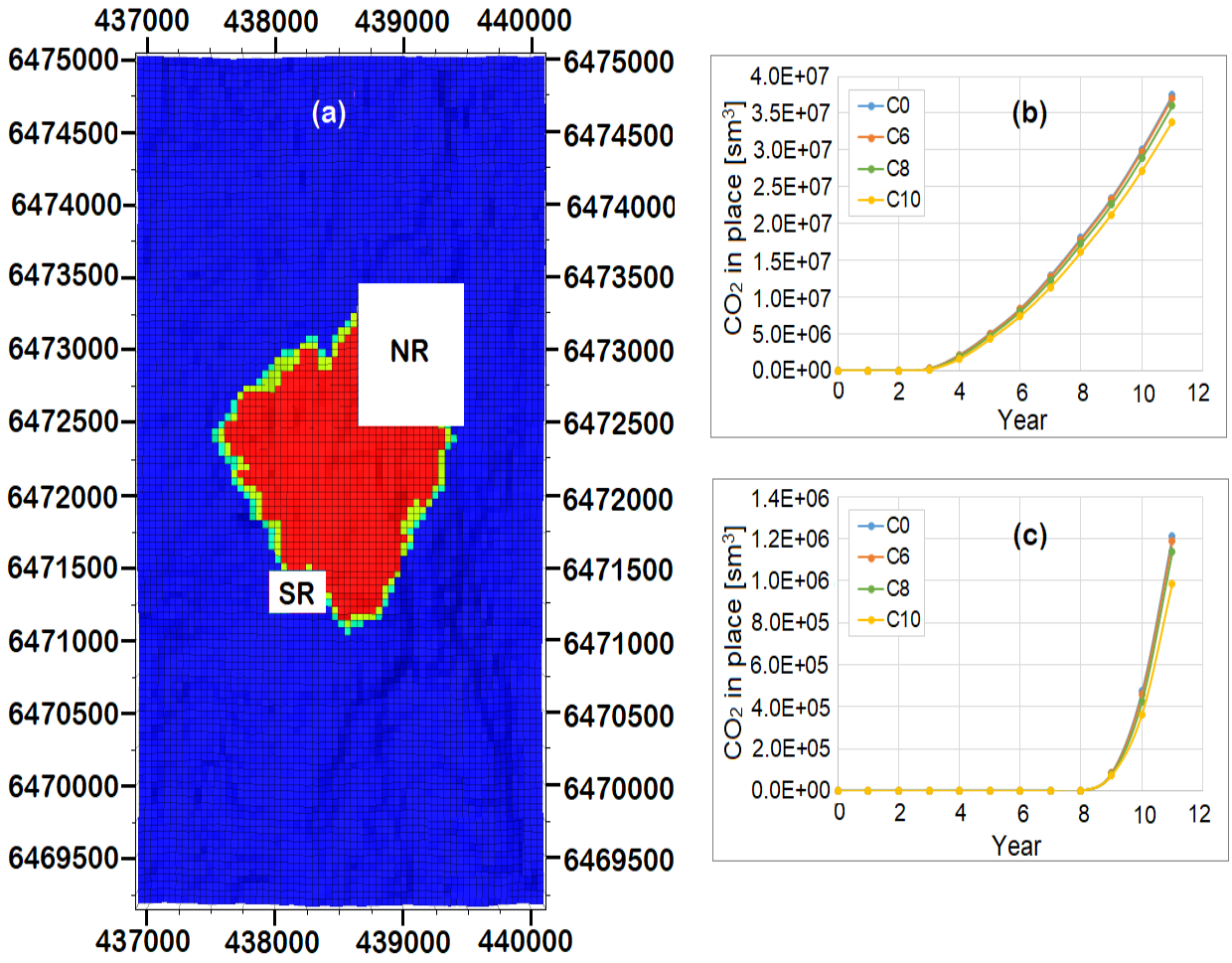

Figure 17: a) The description of the regions in the top layer of the sand wedge where the volume profile of CO_2 is assesed for b) the northern region, NR and c) the southern region, SR, during the simulation period.

Reflecting on 'channelling investigations' by Williams and Chadwick[15] and Cowton et al.,[16] a better calibration of the migration rate at the northern ridge in Darcy flow simulators could be

afforded by introducing heterogeneity in capillary pressure and relative permeability functions incorporated in the top sand wedge. It is common that grid resolution limitations may reduce sensitivity to relative permeability functions and capillary forces in numerical models due to numerical errors. As illustrated by Nilsen et al.,[47] "the large size of coarse grid results in a large difference between the average of the non-linear relative permeability functions and the relative permeability functions evaluated in the average saturation". Refining the simulation grid will help to diminish numerical errors due to poor discretisation. Hence, high-resolution models can be used to easily capture the effects of such functions and support a Darcy-based modelling approach. A downside to using high-resolution models, however, is the computational efficiency of forward modelling within reasonable time scales using full flow physics. This has resulted in the use of less complex simulators and/or analytical methods that adopt a vertically averaged formulation of the governing equations of multiphase flow (e.g. Gasda et al.,[48] Doster et al.,[49] Nielsen et al.,[50] and Cowton et al.[16]). This usually entails modelling the gravity current in its simplest form based on the Vertical Equilibrium (VE) pseudo functions introduced by Coats et al.,[51]. The VE concept assumes gravity forces alone are the driving forces towards equilibrated (segregated) vertical fluid distributions. This implies that the phase hydrostatic potential is independent of depth within a cell and relative permeabilities are calculated using segregated saturation functions in the vertical dimension.[52] This may seem ideal for simulation studies in the Utsira 'sand wedge' since predictions suggest that the plume migration could be primarily buoyancy-driven and not pressure-driven.[18,46] With migration proceeding further away from the injection area, the CO_2 plume becomes thinner, making numerical errors due to poor vertical discretisation more important.[47] Under the assumption that fluid flow predominates in the horizontal direction, VE models utilise the large aspect ratio of CO_2 gravity current to reduce the complexity of flow simulations in 3D and increase computational efficiency.[16]

3.2.2 Gravity-segregated analysis

The cell saturation distribution assumed by ECLIPSE's VE model is based on the assumption that the phase hydrostatic potential is independent of depth. In the absence of capillary pressure effects, the saturation distribution becomes a step function depending on the fluid contact depths. This saturation distribution is taken account of when ECLIPSE calculates relative permeability values for the cell faces.[53] For the gas-water case shown in Figure 18, water may flow out of the bottom of the cell, but not out of the top, at which no mobile water exists. The water flow through the sides reflects the fraction of the cell faces over which a mobile saturation exists. If the VE assumption of approximate hydrostatic equilibrium is valid, such a segregated saturation distribution may provide a more accurate description of fluid flow than a default dispersed option in which the fluids are assumed to be evenly distributed over the grid block.[52]

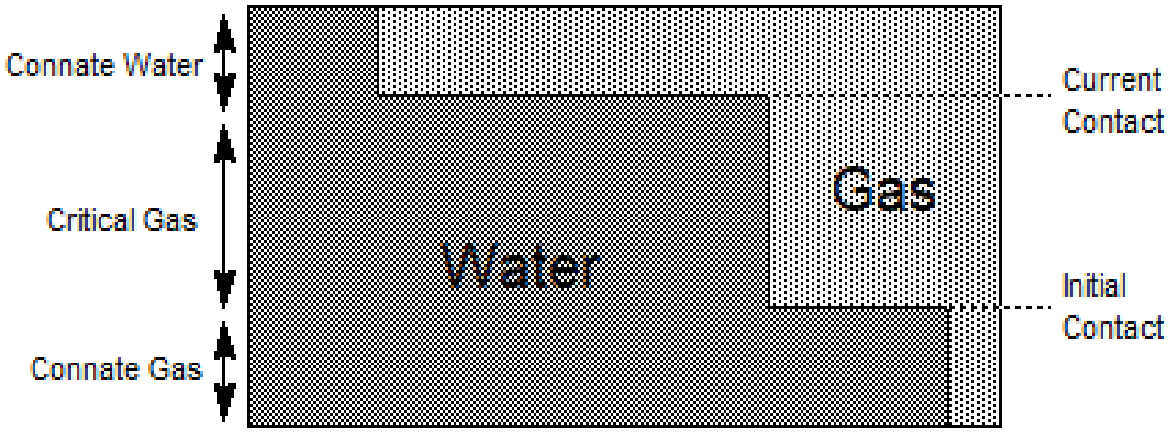

Figure 18: A cell with approximate hydrostatic equilibrium showing gas-water vertical equilibrium

The gravity-segregated flow can be modelled in ECLIPSE using the VE option, where the degree of fluid segregation is specified using mixing parameters 'VEFRAC' and VEFRACP' for the relative permeability and capillary pressure, respectively.[52] These keywords enable the specification of either dispersed (rock curve) or segregated (VE) saturation functions, or a weighted average of the two, for calculating relative permeabilities and capillary pressures. VEFRAC gives the VE relative permeability fraction, and VEFRACP the VE capillary pressure fraction, for the whole field.

Using the VE option, simulation outcome for the sensitivity cases described in Table 5, where relative permeability variations are specified for the rock fabric in high permeability channels, showed no difference to the plume contact area when total fluid segregation is assumed. This is because when VEFRAC equals unity, the simulation disregards the relative permeability curves specified for the rock fabric in high permeability channels and only uses the VE relative permeability curves in the run. However, the VE option allows for an increase in mobility as both phases become relatively mobile in low saturations. The resulting spread in horizontal current becomes a function of the degree of fluid segregation assumed. The higher the degree of fluid segregation, the faster the spread in horizontal current along the topography of the capillary barrier (Figure 19). Figure 20 shows the outline of gas flow in a three-dimensional space where the largest plume contact area is discernible for the assumption of total fluid segregation. Even though the CO_2-water contact in the VE models do not match Sleipner's time-lapse seismic data, they illustrate better northerly and southerly plume distribution than the full Darcy flow physics simulated herein (Figure 21).

The plume distribution trend seen in Figure 21 argues for the value of VE models when calibrating petrophysical properties to history-match the plume spread in Utsira's top sand unit. In the context of sensitivity to relative permeability curves, an assumption of partial fluid segregation when using the VE option in ECLIPSE affords the modelling of CO_2 plume sensitivity to rock curves in the simulation. More importantly, high-resolution modelling using the VE option is computationally efficient. To quote Singh et al.,[18] "as long as high resolution models which include gravity segregation are used, good matches to field observations can be obtained using conventional black-oil simulators".

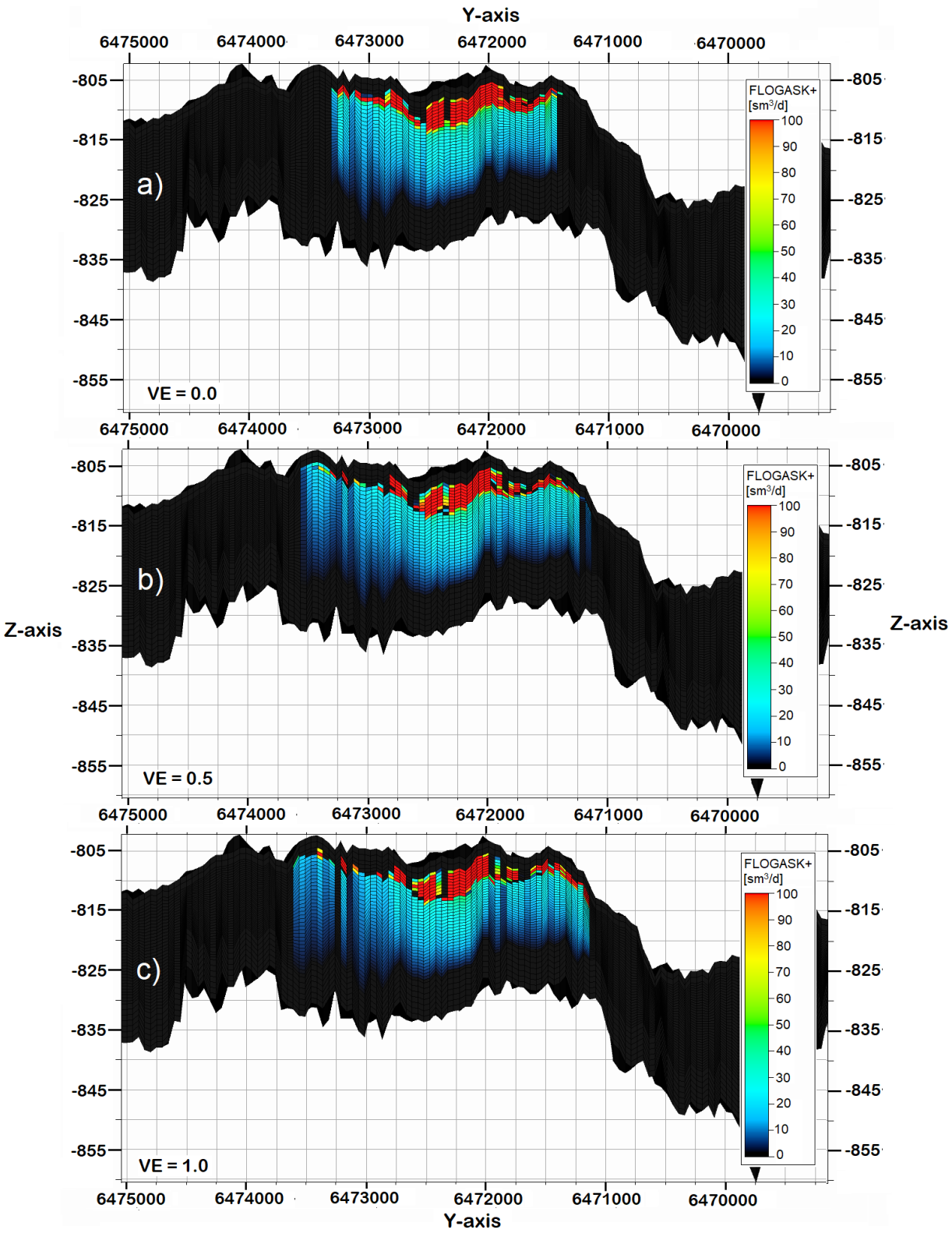

Figure 19: Gravity current in a cross section of the numerical domain for a VE model with a mixing fraction of a) 0.0, b) 0.5 and c) 1.0 at the end of CO_2 injection

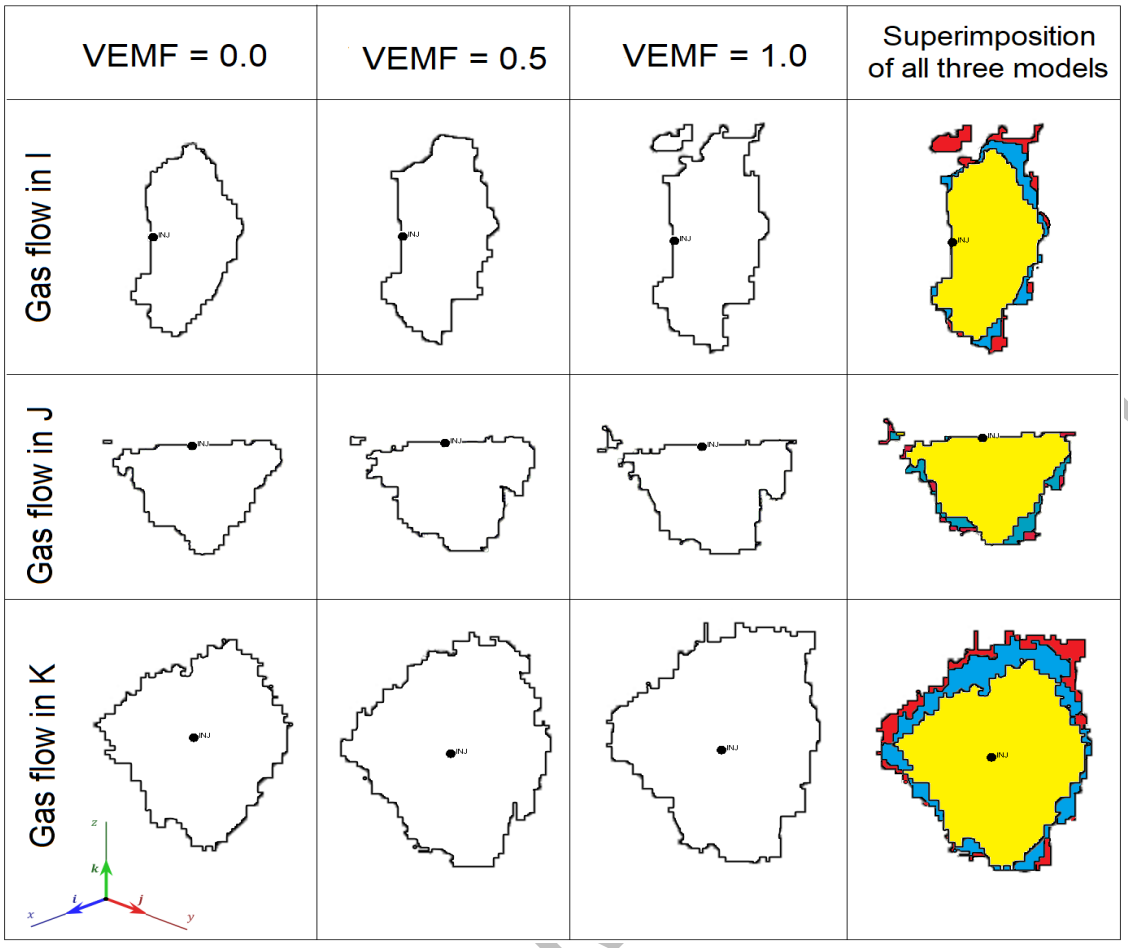

Figure 20: Schematic of saturated gas at the end of simulation in the three-dimensional space for the Vertical Equilibrium Mixing Fraction (VEMF) of 0.0, 0.5 and 1.0 with colour code for superimposed models illustrated as yellow, blue and red, respectively. Black disc indicates the injection point.

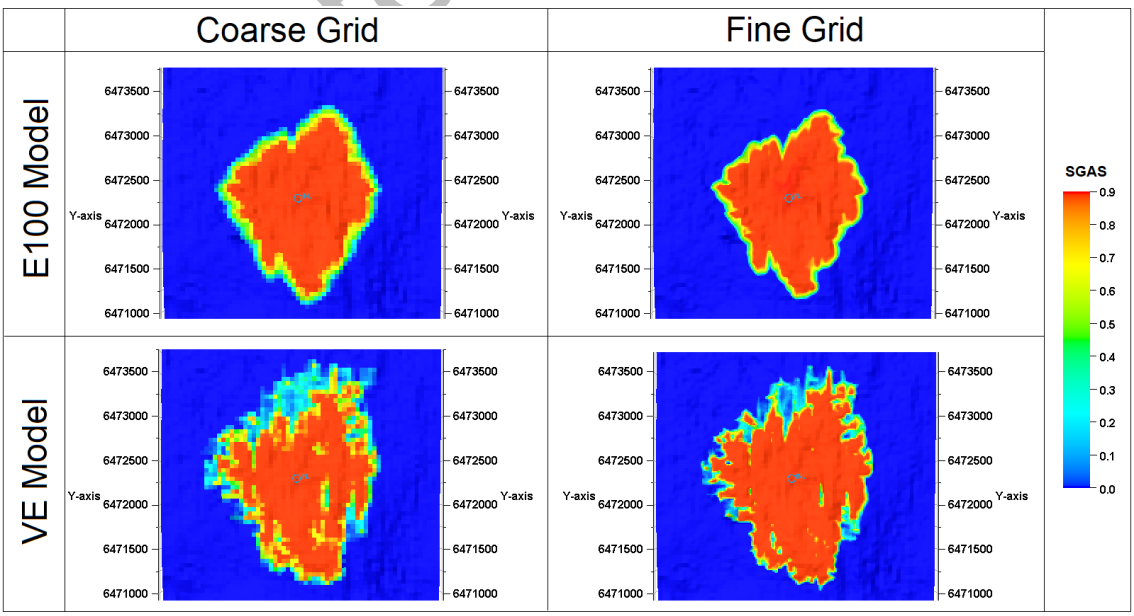

Figure 21: Results of flow simulation in the benchmark model for coarse and fine grids in E100 and VE models

4 Summary and conclusion

The first investigation in this study presented an axisymmetric geometry for a fixed-volume release of supercritical CO_2 into a saline formation with intra-sand mudstone baffles in cases that describe drainage of the fluid through:

i) Viscous-limit pathways in the interbedded mudstone layers, and

ii) Capillary-limit percolation in semi-permeable mudstone layers.

The models developed were simplified but provided valuable insight into the effects of relative permeability and capillary functions on the propagation of gravity-dominated displacement flow in porous rocks. The flow modelling approach presented here suggest that the semi-permeable thin argillite layers have an atypically low capillary entry pressure of 1.72 KPa that enables the rapid vertical migration of CO_2 from the base to the top of the reservoir formation. The possibility of such low threshold pressures has been attributed to the occurrence of micron-fractures in the argillite layer, probably induced, prior to CO_2 injection, by transient fluid overpressure during rapid deglaciation at Sleipner.[17] The local capillary forces and relative permeability to the invading fluid were found to play a key role in moderating the rate of buoyant migration through the reservoir, including buoyant migration through pathways in laterally extensive mudstone layers. Results show that capillary forces within semi-permeable barriers in a storage formation regulates the degree of CO_2 mass that breaches the capillary barriers, while the rate of leakage in the gravity current passing through the barrier is a function of its relative permeability to the invading fluid.

The second investigation considered the sensitivity of plume extension to relative permeability functions in flow channels within the top sand unit of Utsira Formation. This assumed visco-capillary Darcy flow as the dominant process in modelling the distribution of CO_2 in the Sleipner benchmark model. Simulation outcome was found to vary from the observed CO_2-water contact in the seismic data. The poor performance of Darcy flow physics to simulate seismically-observed fluxes at the Utsira Formation, e.g. Chadwick et al.,[42] Hermanrud et al.,[43] Singh et al.,[18] and

Cavanagh,[46] has been attributed to the underlying governing equation of Darcy's law which requires pressure gradient-driven viscous flow in permeable media. Nevertheless, Cavanagh[46] observed that a pressure-compensated modelling approach improves the performance of Darcy flow models in matching the observed distribution of CO_2 at Sleipner. Most importantly, incorporating detailed depositional heterogeneity of the top sand wedge into Darcy flow models have resulted in a closer history match in CO_2 plume distribution.[15] However, including heterogeneity in relative permeability and capillary functions when modelling depositional heterogeneity is easily overlooked in the simulation of CO_2 geo-sequestration. Although the sensitivity of the CO_2 plume morphology, particularly within the channels in the top sand wedge, to relative permeability functions seemed insignificant in this study, including relative permeability heterogeneity in simulation studies, where and when applicable, should not be ignored. This is because the introduction of relative permeability variations opens up the possibility of investigating uncertainties for fluid flow in model space by facilitating a Darcy modelling approach.

Acknowledgements

This paper is based upon work supported by Coventry University's Fluid and Complex Systems Research Centre. We thank Equinor and the Sleipner licence partners for the permission to use the dataset discussed in this paper. We acknowledge Gareth Williams (British Geological Survey) for providing the fluid properties for the black oil simulation, and Schlumberger for the use of ECLIPSE and Petrel Software.

References

1. Honarpour, M. M. *et al. Integrated methodology for constructing a quantified hydrodynamic model for application to clastic petroleum reservoirs*. (1990). doi:NIPER-439 (DE 9000211)
2. Bear, J. *Dynamics of Fluids in Porous Media*. (American Elsevier Publishing Company,

1972).

3. Al-Menhali, A. *et al.* Advanced Reservoir Characterization for CO2 Storage. in *International Petroleum Technology Conference* (International Petroleum Technology Conference, 2014). doi:10.2523/IPTC-17253-MS

4. Haldorsen, H. . & Damsleth, E. Challenges in Reservoir Characterization. *Am Assoc Pet Geol Bull* **77,** 541–551 (1993).

5. Fertl, W. H. & Chilingarian, G. V. Type and distribution modes of clay minerals from well logging data. *J Pet Sci Eng* **3,** 321–332 (1990).

6. Arts, R. *et al.* Monitoring of CO2 injected at Sleipner using time-lapse seismic data. *Energy* **29,** 1383–1392 (2004).

7. Zweigel, P., Arts, R., Lothe, A. E. & Lindeberg, E. B. G. Reservoir geology of the Utsira Formation at the first industrial-scale underground CO2 storage site (Sleipner area, North Sea). *Geol Soc London, Spec Publ* **233,** 165–180 (2004).

8. Chadwick, R. A., Arts, R. & Eiken, O. 4D seismic quantification of a growing CO2 plume at Sleipner, North Sea. *Geol Soc London, Pet Geol Conf Ser* **6,** 1385–1399 (2005).

9. Chadwick, R. A. *et al.* 4D Seismic Imaging of an Injected CO2 Plume at the Sleipner Field, Central North Sea. *Geol Soc London, Mem* **29,** 311–320 (2004).

10. Chadwick, R. A. & Noy, D. J. History-matching flow simulations and time-lapse seismic data from the Sleipner CO2 plume. *Geol Soc London, Pet Geol Conf* **7,** 1171–1182 (2010).

11. Cowton, L. R. *et al.* An inverse method for estimating thickness and volume with time of a thin CO2-filled layer at the Sleipner Field, North Sea. *J Geophys Res Solid Earth* **121,** 5068–5085 (2016).

12. Harrington, J. F., Noy, D. J., Horseman, S. T., Birchall, D. J. & Chadwick, R. A. Laboratory Study of Gas and Water Flow in the Nordland Shale, Sleipner, North Sea. in

Carbon dioxide sequestration in geological media--state of the science (eds. Grobe, M., Pashin, J. C. & Dodge, R. L.) 521–543 (AAPG Special Volumes, 2009). doi:10.1306/13171259ST593394

13. Hermanrud, C., Zweigel, P., Eiken, O., Lippard, J. & Andresen, T. CO2 flow in the Utsira Formation: Inferences made from 4D seismic analysis in the Sleipner area. in *European Conference of the American Association of Petroleum Geologists* (2007).
14. Boait, F., White, N., Chadwick, A., Noy, D. & Bickle, M. Layer spreading and dimming within the CO2 plume at the sleipner field in the north sea. *Energy Procedia* **4,** 3254–3261 (2011).
15. Williams, G. A. & Chadwick, R. A. An Improved History-match for Layer Spreading within the Sleipner Plume Including Thermal Propagation Effects. *Energy Procedia* **114,** 2856–2870 (2017).
16. Cowton, L. R. *et al.* Benchmarking of vertically-integrated CO2 flow simulations at the Sleipner Field, North Sea. *Earth Planet Sci Lett* **491,** 121–133 (2018).
17. Cavanagh, A. J. & Haszeldine, R. S. The Sleipner storage site: Capillary flow modeling of a layered CO2 plume requires fractured shale barriers within the Utsira Formation. *International Journal of Greenhouse Gas Control* **21,** 101–112 (2014).
18. Singh, V. P. *et al.* Reservoir Modeling of CO2 Plume Behavior Calibrated Against Monitoring Data From Sleipner, Norway. in *SPE Annual Technical Conference and Exhibition* (Society of Petroleum Engineers, 2010). doi:10.2118/134891-MS
19. Bickle, M., Chadwick, A., Huppert, H. E., Hallworth, M. & Lyle, S. Modelling carbon dioxide accumulation at Sleipner: Implications for underground carbon storage. *Earth Planet Sci Lett* **255,** 164–176 (2007).
20. Chadwick, R. A., Williams, G. A., Williams, J. D. O. & Noy, D. J. Measuring pressure performance of a large saline aquifer during industrial-scale CO2 injection: The Utsira

Sand, Norwegian North Sea. *Int J Greenh Gas Control* **10,** 374–388 (2012).

21. Zhang, G., Lu, P., Ji, X. & Zhu, C. CO2 Plume Migration and Fate at Sleipner, Norway: Calibration of Numerical Models, Uncertainty Analysis, and Reactive Transport Modelling of CO2 Trapping to 10,000 Years. *Energy Procedia* **114,** 2880–2895 (2017).
22. Gaus, I., Azaroual, M. & Czernichowski-Lauriol, I. Reactive transport modelling of the impact of CO2 injection on the clayey cap rock at Sleipner (North Sea). *Chem Geol* **217,** 319–337 (2005).
23. White, J. C., Williams, G., Chadwick, A., Furre, A.-K. & Kiær, A. Sleipner: The ongoing challenge to determine the thickness of a thin CO2 layer. *Int J Greenh Gas Control* **69,** 81–95 (2018).
24. Dupuy, B. *et al.* Quantitative seismic characterization of CO2 at the Sleipner storage site, North Sea. *Interpretation* **5,** SS23-SS42 (2017).
25. Ghosh, R., Sen, M. K. & Vedanti, N. Quantitative interpretation of CO2 plume from Sleipner (North Sea), using post-stack inversion and rock physics modeling. *Int J Greenh Gas Control* **32,** 147–158 (2015).
26. Chadwick, R. A. & Noy, D. J. Underground CO_2 storage: demonstrating regulatory conformance by convergence of history-matched modeled and observed CO_2 plume behavior using Sleipner time-lapse seismics. *Greenh Gases Sci Technol* **5,** 305–322 (2015).
27. Romdhane, A., Querendez, E. & Ravaut, C. CO2 Thin-layer Detection at the Sleipner Field with Full Waveform Inversion: Application to Synthetic and Real Data. *Energy Procedia* **51,** 281–288 (2014).
28. Zhu, C., Zhang, G., Lu, P., Meng, L. & Ji, X. Benchmark modeling of the Sleipner CO2 plume: Calibration to seismic data for the uppermost layer and model sensitivity analysis. *Int J Greenh Gas Control* **43,** 233–246 (2015).

29. Juanes, R., Spiteri, E. J., Orr, F. M. & Blunt, M. J. Impact of relative permeability hysteresis on geological CO2 storage. *Water Resour Res* **42,** 1–13 (2006).

30. Burnside, N. M. & Naylor, M. Review and implications of relative permeability of CO2/brine systems and residual trapping of CO2. *International Journal of Greenhouse Gas Control* **23,** 1–11 (2014).

31. Onoja, M. U. & Shariatipour, S. M. The impact of gradational contact at the reservoir-seal interface on geological CO<inf>2</inf> storage capacity and security. *Int J Greenh Gas Control* **72,** (2018).

32. Onoja, M. U., Ahmadinia, M., Shariatipour, S. M. & Wood, A. M. Characterising the role of parametric functions in the van Genuchten empirical model on CO2 storage performance. *Int J Greenh Gas Control* **88,** 233–250 (2019).

33. Van Genuchten, M. T. A closed form equation for predicting the hydraulic conductivity of unsaturated soils. *Soil Sci Soc Am J* **44,** 892–898 (1980).

34. Deuflhard, P. (Peter). *Newton methods for nonlinear problems : affine invariance and adaptive algorithms*. (Springer, 2004).

35. Schlumberger. *ECLIPSE UserGuide*. (2017).

36. Schlumberger. *ECLIPSE Reference Manual*. (2017).

37. Haukaas, J., Nickel, M. & Sonneland, L. Successful 4D History Matching of the Sleipner CO2 Plume. in *75th EAGE Conference & Exhibition incorporating SPE EUROPEC 2013* (EAGE, 2013). doi:10.3997/2214-4609.20130820

38. van Genuchten, M. T. & Nielsen, D. R. On Describing and Predicting the Hydraulic Properties of Unsaturated Soils. *Ann Geophys* **3,** 615–628 (1985).

39. Mualem, Y. A new model for predicting the hydraulic conductivity of unsaturated porous media. *Water Resour Res* **12,** 513–522 (1976).

40. Williams, G. A., Chadwick, R. A. & Vosper, H. Some thoughts on Darcy-type flow

simulation for modelling underground CO2 storage, based on the Sleipner CO2 storage operation. *Int J Greenh Gas Control* **68,** 164–175 (2018).

41. Odsæter, L. H., Berg, C. F. & Rustad, A. B. Rate Dependency in Steady-State Upscaling. *Transp Porous Media* **110,** 565–589 (2015).

42. Chadwick, A. *et al.* Calibrating reservoir performance with time-lapse seismic monitoring and flow simulations of the Sleipner CO2 plume. in *GHGT-8: 8th International Conference on Greenhouse Gas Control Technologies, 19-22 June 2006* 1–6 (Elsevier, 2006).

43. Hermanrud, C. *et al.* Storage of CO2 in saline aquifers–Lessons learned from 10 years of injection into the Utsira Formation in the Sleipner area. *Energy Procedia* **1,** 1997–2004 (2009).

44. Hobson, G. D. *Some fundamentals of petroleum geology*. (Oxford University Press, 1954).

45. Cavanagh, A. & Nazarian, B. A new and extended Sleipner Benchmark model for CO2 storage simulations in the Utsira Formation. *Energy Procedia* **63,** 2831–2835 (2014).

46. Cavanagh, A. Benchmark Calibration and Prediction of the Sleipner CO2 Plume from 2006 to 2012. *Energy Procedia* **37,** 3529–3545 (2013).

47. Nilsen, H. M. *et al.* Field-case simulation of CO2 -plume migration using vertical-equilibrium models. *Energy Procedia* **4,** 3801–3808 (2011).

48. Gasda, S. E., Nordbotten, J. M. & Celia, M. A. Vertical equilibrium with sub-scale analytical methods for geological CO2 sequestration. *Comput Geosci* **13,** 469–481 (2009).

49. Doster, F., Nordbotten, J. M. & Celia, M. A. Impact of capillary hysteresis and trapping on vertically integrated models for CO2 storage. *Computational Methods in Geologic CO2 Sequestration* **62,** 465–474 (2013).

50. Nilsen, H. M., Krogstad, S., Andersen, O., Allen, R. & Lie, K.-A. Using Sensitivities and Vertical-equilibrium Models for Parameter Estimation of CO2 Injection Models with

Application to Sleipner Data. *Energy Procedia* **114,** 3476–3495 (2017).

51. Coats, K. H., Dempsey, J. R. & Henderson, J. H. The Use of Vertical Equilibrium in Two-Dimensional Simulation of Three-Dimensional Reservoir Performance. *Soc Pet Eng J* **11,** 63–71 (1971).

52. Schlumberger. *ECLIPSE Technical Description*. (2017).

53. Ahmadinia, M., Shariatipour, S. M., Andersen, O. & Sadri, M. Benchmarking of vertically integrated models for the study of the impact of caprock morphology on CO2 migration. *Int J Greenh Gas Control* **90,** 102802 (2019).

CASE ID	Description
P0	Presence of capillary forces in the intra-sand mudstones; Pathway in the mudstones based on intrinsic permeability value of 70 mD and $P_c - k_r - S_w$ function for reservoir sand (where the capillary pressure, P_e, is 1.72 KPa, the residual wetting saturation, S_w, is 0.3 and pore geometry parameter, m, is 0.56).
P1	Presence of capillary forces in the intra-sand mudstones; Pathway based on only intrinsic permeability value of 70 mD.
P2	Absence of capillary forces in the intra-sand mudstones; Pathway based on intrinsic permeability value of 70 mD.
P3	Absence of capillary forces in the intra-sand mudstones; Pathway based on intrinsic permeability value of 70 mD and $k_r - S_w$ function for reservoir sand, where $P_c = 0$.
P4	Presence of capillary forces in the intra-sand mudstones; Pathway based on only $P_c - k_r - S_w$ function for reservoir sand.
P5	Presence of capillary forces in the intra-sand mudstones; No pathway – Flow properties of thin argillites are the same as the caprock.

Table 1: Description of cases modelled for pathway flow analysis

Argillaceous unit	Pore-geometry parameter [m]
Sandy Siltstone	0.29
Siltstone	0.27
Mudstone	0.24
Sandy Claystone	0.19
Claystone/Caprock	0.08

Table 2: Descriptive m-value in van Genuchten model for the argillaceous units. [Adapted from Onoja et al.,[32]].

Case ID	Description of intra-sand argillite layers M1 – M6
S0	All Sandy Siltstone
S1	All Siltstone
S2	All Mudstone
S3	According to plume thickness in the 2001 Sleipner data set (Figure 2b) under the following assumptions: M1 = Sandy Siltstone, M2 = Siltstone, M3 = Mudstone, M4 = Sandy Siltstone, M5 = Sandy Claystone, and M6 = Siltstone.

Table 3: Description of sensitivity cases modelled for capillary-dominated Darcy flow analysis. NB: $P_c - k_r - S_w$ description for M7 is equivalent to the 'sandy siltstone' for all cases modelled.

Parameter	***Value***
Pore geometry parameter [m]	0.95
Brine relative permeability end-point	0.54
CO_2 relative permeability end-point	0.75
Critical brine saturation	0.386
Connate brine saturation	0.11
Critical CO_2 saturation	0.02
Connate CO_2 saturation	0.00
Permeability of the sand wedge [mD]	2000
Permeability anisotropy	0.1
Porosity of the sand wedge sand	0.36

Table 4: Parameters used for the simulation of Sleipner Layer 9 in this study.

Case ID	*Description of 'thief zones'*
C0	Base case where $m = 0.95$
C1	$m = 0.96$
C2	$m = 0.97$
C3	$m = 0.98$
C4	$m = 0.99$
C5	$m = 0.91$
C6	$m = 0.85$
C7	$m = 0.81$
C8	$m = 0.75$
C9	$m = 0.71$
C10	$m = 0.65$

Table 5: Description of cases that investigate the sensitivity of temporal evolution of CO_2 in the topmost layer to relative permeability functions in the high permeability channels.